ANL-6854
Engineering and
Equipment
(TID-4500, 30th Ed.)
AEC Research and
Development Report

ARGONNE NATIONAL LABORATORY
9700 South Cass Avenue
Argonne, Illinois 60440

EFFECT OF A TRANSVERSE MAGNETIC FIELD ON VERTICAL TWO-PHASE FLOW THROUGH A RECTANGULAR CHANNEL

by

Richard J. Thome

Reactor Engineering Division
and
Associated Midwest Universities

March 1964

Reproduced from Thesis Submitted in Partial Fulfillment of the Requirements for the Degree of Master of Mechanical Engineering in the Graduate School of Syracuse University

Operated by The University of Chicago
under
Contract W-31-109-eng-38
with the
U. S. Atomic Energy Commission

DISCLAIMER

FOREWORD

This report is one of a series that describes heat-transfer and fluid-flow studies performed at Argonne under a program sponsored jointly by the Associated Midwest Universities and the Argonne National Laboratory.

The earlier reports in this series are:

ANL-6625 Local Parameters in Cocurrent Mercury-Nitrogen Flow
L. G. Neal

ANL-6667 A Study of the Flow of Saturated Freon-11 through Apertures and Short Tubes
Hans K. Fauske and Tony C. Min

ANL-6674 Reduction of Vapor Carryunder in Simulated Boiling
P. L. Miller and C. P. Armstrong

ANL-6710 Transient Behavior of a Natural-Circulation Loop Operating Near the Thermodynamic Critical Point
Darrel G. Harden

ANL-6734 Two-phase (Gas-liquid) System: Heat Transfer and Hydraulics. An Annotated Bibliography
Robert R. Kepple and Thomas V. Tung

ANL-6738 Development of an Electrical Resistivity Probe for Void-fraction Measurements in Air-Water Flow
George P. Nassos

ANL-6754 An Experimental Investigation of Two-phase, Two-component Flow in a Horizontal, Converging-diverging Nozzle
Joseph A. Vogrin, Jr.

ANL-6755 Two-component Two-phase Flow Parameters for Low Circulation Rates
Georges E. Smissaert

ANL-6779 Two-phase Critical Flow with Application to Liquid-Metal Systems (Mercury, Cesium, Rubidium, Potassium, Sodium, and Lithium)
Hans K. Fauske

ANL-6796 The Slug-annular Flow Regime Transition at Elevated Pressure
Peter Griffith

TABLE OF CONTENTS

LIST OF FIGURES

LIST OF FIGURES

LIST OF FIGURES

EFFECT OF A TRANSVERSE MAGNETIC FIELD ON VERTICAL TWO-PHASE FLOW THROUGH A RECTANGULAR CHANNEL

by

Richard J. Thome

ABSTRACT

A study was undertaken to determine the effects of the magnetic field on: (1) distribution of gas in the field direction, (2) slip ratio, and (3) two-phase pressure drop. Metered streams of sodium-potassium alloy (NaK) and nitrogen were mixed and pumped through a vertical, constant-area, rectangular channel with a transverse magnetic field applied perpendicularly to the long side of the cross section. This system was comparable to a liquid metal magnetohydrodynamic generator operating on open circuit with a two-phase, two-component mixture as the working fluid.

The results are briefly as follows:

1. The magnetic field tended to make the gas distribution more uniform. There was no observable tendency for the field to shift the gas to either side of the channel in the direction of the imposed field.

2. The effect of the magnetic field was to increase slip ratio in all cases.

3. The magnetic field was observed to virtually nullify the tendency for the introduction of a gaseous phase to greatly increase pressure drop above the single phase value at the same liquid flow rate. This effect was predicted reasonably well by a magnetic, two-phase, friction-factor multiplier which was based on a simplified model.

I. INTRODUCTION

In recent years, it has become apparent that a lightweight, reliable, electric power-producing system is required as one of the steps toward a successful probe into space. To meet this requirement certain systems have been proposed which would yield a nuclear to electric power conversion without the use of moving mechanical parts.

One such group of systems is based on the heating of a working fluid to the plasma state and utilizing it as the moving conductor in a magnetohydrodynamic (MHD) generator. However, the reactor temperatures required for a light and efficient system of this type are prohibitively high. This realization led to the proposal of certain cycles which would lower the required temperature by using two working fluids, a gas for the thermal to kinetic conversion, and a conducting liquid (liquid metal) for the kinetic to electric conversion. An example of a cycle of this type proposed by Elliott[9] is shown in Fig. 1.

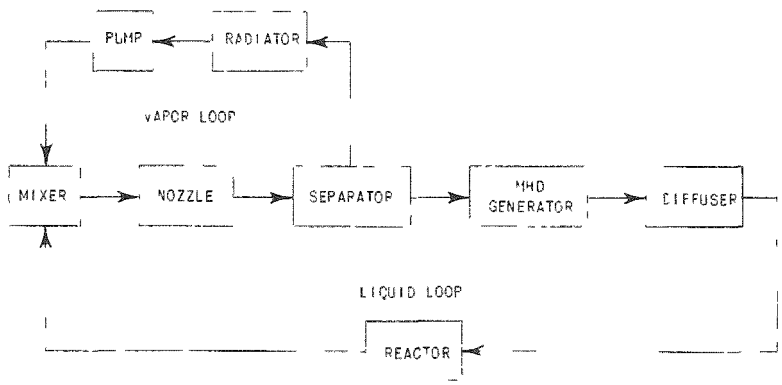

Fig. 1. Two-fluid MHD Cycle for Nuclear Electric Power Conversion[9]

Together with analyses as to the theoretical feasibility of such systems, experiments must be conducted to determine the performance characteristics of cycle components. In the cycle shown in Fig. 1, incomplete liquid-vapor separation would result in a two-phase mixture passing through the generator. A step toward understanding the generator characteristics in this situation is therefore a determination of the effects of a magnetic field on two-phase flow phenomena, in particular, on pressure drop and void fraction. In this study, the observed effects are comparable with those occurring in a liquid metal MHD generator operating on open circuit with a two-phase, two-component mixture as the working fluid.

For certain liquid metals, including the sodium-potassium alloy (~78% potassium, 22% sodium) used in this study, the single-phase pressure drop under normal fluid flow conditions may be calculated by application of methods used for more familiar fluids.[8] The hydraulic similarity which makes this possible also allows comparison of flow phenomena involving two phases of fluid.

In contrast, the flow characteristics of common fluids and of liquid metals are not similar in the presence of a magnetic field. The main cause for this difference in reaction is the relatively high electrical conductivity of liquid metals (e.g., the conductivity of sodium-potassium alloy is higher by approximately four orders of magnitude than that of the best electrolyte).[1]

This leads to the induction of relatively large electromagnetic forces, which alter the character of the flow.

A great deal of work has been done on the flow of single-phase fluids through a magnetic field. A summary may be found in Shercliff[1] which also contains an extensive bibliography. To the author's knowledge, there is no published information on the effects of a magnetic field on two-phase pressure drop and void fraction.

The objectives of the study described herein were: (1) to determine the effect of the magnetic field on the void profile in a plane parallel to the direction of flow and to the direction of the applied magnetic field; (2) to investigate the effect of the magnetic field on slip ratio (the ratio of the average gas velocity to average liquid velocity at a given cross section); (3) to determine the effect of the magnetic field on two-phase pressure drop.

In addition, single-phase pressure-drop data were procured to provide information which, when compared with present or future developments in single-phase theory, would serve as a starting point for the theoretical understanding of the observed two-phase phenomena.

II. EXPERIMENTAL APPARATUS

A. General

Two-phase phenomena were studied under three conditions of constant magnetic field strength: 0, 4300, and 7840 Gauss, and two conditions of NaK flow rate: 14.5 and 50 lb/min (corresponding to average single-phase velocities through the test section of 1.27 ft/sec and 4.37 ft/sec, respectively). Thus, six sets of data were obtained. Each set represented a condition of constant NaK flow rate and constant magnetic field strength with nitrogen flow rate varying to provide average void fraction of from 0 to approximately 65 per cent.

Measurements of void distribution were made upstream and downstream of the magnetic field for each. The direction of traverse was perpendicular to the flow and parallel to the magnetic field. Traverse positions were between the ends of the field poles and corresponding upstream and downstream pressure taps of the test section (see Fig. 10).

Three groups of pressure-drop data were obtained for each of the aforementioned test conditions, each group consisting of pressure drop between (see Fig. 10): (1) points 1 and 3, i.e., including the entire field region; (2) points 1 and 2, i.e., the first half of the imposed field region; (3) points 2 and 3, i.e., the last half of the imposed field region.

Single-phase pressure-drop tests were conducted under six conditions of constant magnetic field strength: 0, 4300, 6370, 7280, 7840, and 8270 Gauss. NaK flow rates were varied from the maximum possible under the given field condition to approximately 15 lb/min. Three groups of pressure-drop data as mentioned above were also taken for each field strength under single-phase conditions.

In Fig. 2 the loop used for this study is schematically represented. Metered streams of NaK and dry nitrogen were combined by the gas injector. After passing through the test section, the two-phase stream entered the separator, where the nitrogen was removed and expelled to the atmosphere. The NaK flowed to the expansion tank and on to the pump. The dump tanks served as storage tanks for the NaK when the loop was not in operation, as well as a safety feature in the event of an emergency.

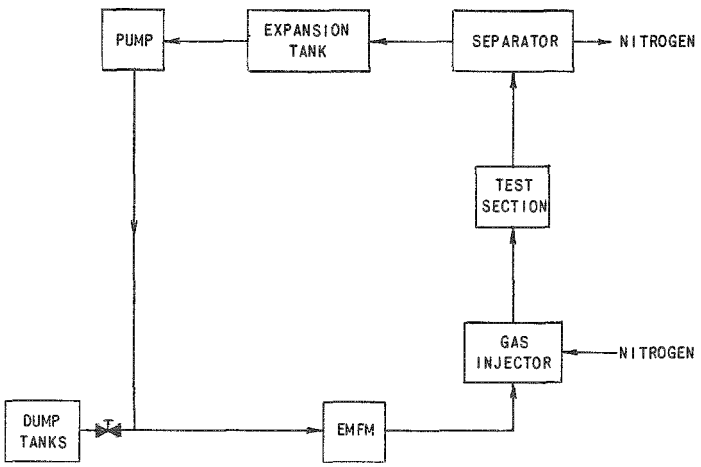

Fig. 2

Experimental Loop

Physically, the entire loop and instrumentation occupied a space 25 ft long, 18 ft high and 9 ft wide. The basic flow system was constructed from 2-in., Schedule 40 stainless steel pipe with stainless steel bellows-sealed globe valves. Loop components were of a welded stainless steel design.

Operational gas requirements were met by three independent nitrogen systems: one to supply nitrogen to the gas injector, one to provide for the shaft-sealing arrangement on the pump,[1] one to provide a blanket gas for the system and to pressurize the dump tanks to fill the system.

B. Loop Components

1. NaK Pump

The NaK pump, represented schematically in Fig. 3 and depicted photographically in Fig. 4, was of the vertically mounted centrifugal type, directly driven by a three-phase, $\frac{3}{4}$-hp motor.

[1]See Loop Components, NaK Pump, this page.

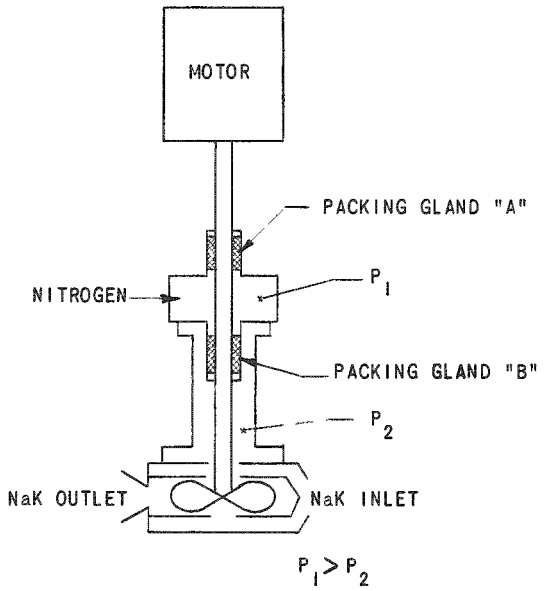

Fig. 3. Diagram of NaK Pump

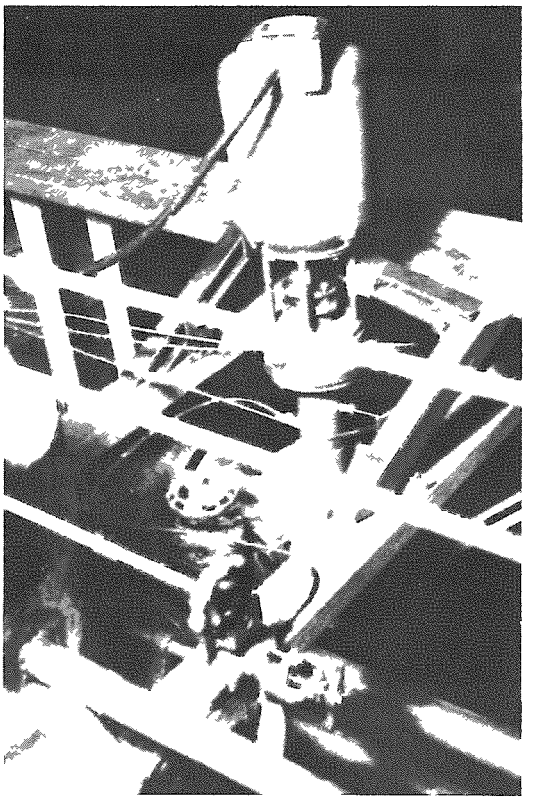

112-3497

Fig. 4. NaK Pump

NaK was prevented from reaching the atmosphere by maintaining a 0.5- to 1-psi differential between the high- and low-pressure sections (see Fig. 3; $P_1 - P_2 \approx 1$ psi). The low pressure was that of the system blanket gas, i.e., approximately 1 psig. These high and low pressures, as well as the breather-tank[2] pressure and dump-tank pressure, were indicated by compound bourdon tube gages which had been calibrated against a mercury manometer.

Shaft seals A and B were of the packing gland type with an asbestos-graphite packing. Nitrogen leaked to the atmosphere through gland A. The introduction of gas to the NaK stream via gland B was considered negligible, since no voids were detected in the test section when the system was operated with no nitrogen supplied to the gas injector.

NaK flow rates were adjusted with a valve located between the electromagnetic flowmeter and the gas injector.

2. Electromagnetic Flowmeter

An electromagnetic flowmeter was constructed by mounting a permanent magnet on a suitable section of a straight pipe and welding

[2]See Loop Components, NaK-Nitrogen Separator, p. 13.

two electrodes to the pipe such that the electrodes were perpendicular to the pipe and to the magnetic field.

The output of the flowmeter was fed through a 10-to-1 amplifier to a Brown recorder.

The flowmeter was calibrated against a sharp-edged orifice introduced in the system by alteration of flowpath. Calibration on two separate occasions over different flow ranges indicated the expected linear approximation of flowmeter output vs flow rate.

The characteristics of the orifice were calculated with flow coefficients determined according to ASME specifications.(5) The limits of accuracy of the electromagnetic flowmeters are usually taken to be ±5%.[3]

3. Gas Injector; Supply and Metering System

The gas injector, shown schematically in Fig. 5, consisted essentially of a short length of perforated 2-in. stainless steel pipe surrounded by a concentric length of 5-in. pipe. The annulus was blanked off at each end.

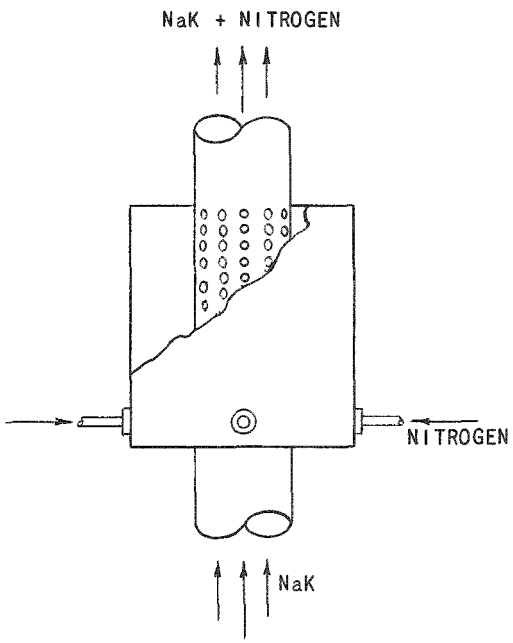

Fig. 5. Gas Injector

Nitrogen entered the chamber through four radially spaced, $\frac{1}{4}$-in., stainless steel tubes. The gas was then able to enter the vertically flowing NaK stream through 165 holes spaced around and along the inner cylinder.

The gas was supplied by standard "bottles" and fed through one of two parallel sharp-edged orifices to a manifold which distributed the nitrogen to the four tubes leading to the injector. This system is schematically represented in Fig. 6.

The characteristics of the orifices were calculated with flow coefficients obtained from a study of small-diameter orifices by Grace and Lapple.(6) Pressure drop across the orifices was determined with a 0- to 5-psid Statham transducer, the output of which was fed to a Brown recorder. The transducer was initially calibrated against a mercury manometer with an accuracy of approximately 0.1 in. Hg.

---

[3] J. A. Shercliff, The Theory of Electromagnetic Flow Measurement, Cambridge University Press (1962), p. 108.

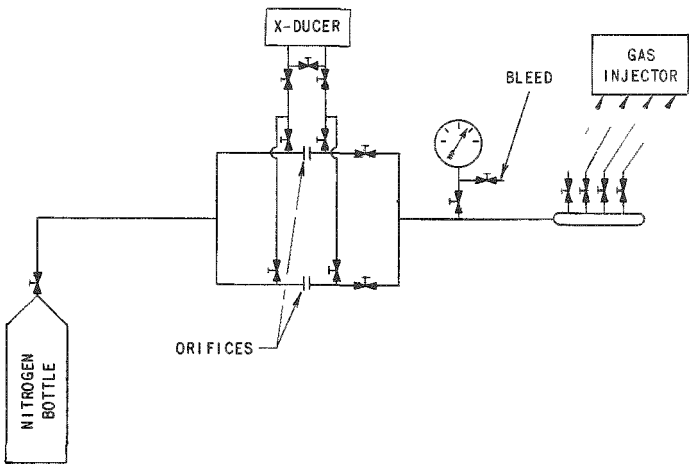

Fig. 6

Gas-injector Supply and Metering System

4. NaK-Nitrogen Separator

The separator, shown schematically in Fig. 7 and photographically in Fig. 8, consisted of a relatively large cylindrical tank mounted at a slight angle to the horizontal. The tank was of large capacity to allow the incoming two-phase mixture to decrease velocity and give up its gas by natural density-difference phenomena.

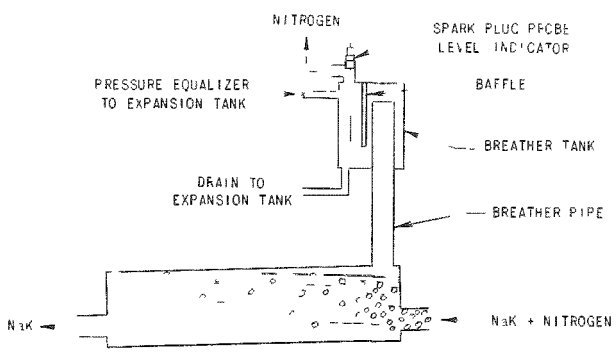

Fig. 7. Schematic Representation of NaK-Nitrogen Separator

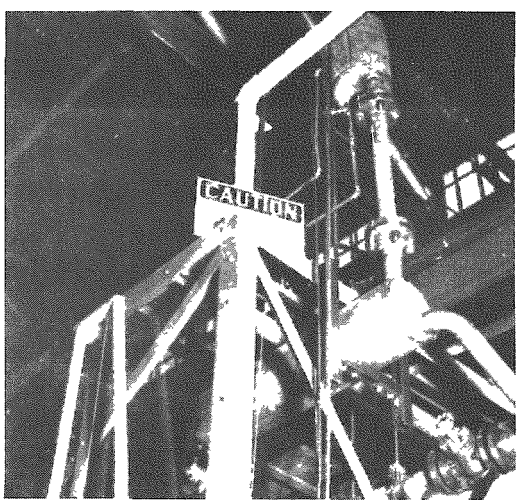

112-3495

Fig. 8. NaK-Nitrogen Separator

The breather tank was provided with a pressure-equalizing line to the expansion tank to maintain a relatively constant NaK level between the separator and expansion tank. In addition, a drain line to the expansion tank was added to serve in the event of NaK carryover by the breather pipe. A baffle prevented NaK from splashing into the equalizing and bleed lines, and a spark plug-type level indicator tripped an alarm if NaK accumulated in the tank.

5. Expansion Tank

The large tank illustrated in Fig. 9 was located in the flowpath between the separator and pump. In this study, NaK entered the bottom of the tank, passed around baffles which prevented splashing, and continued to the pump through an outlet at the rear. Observation ports served as a visual indicator of liquid level when in operation and when filling the system.

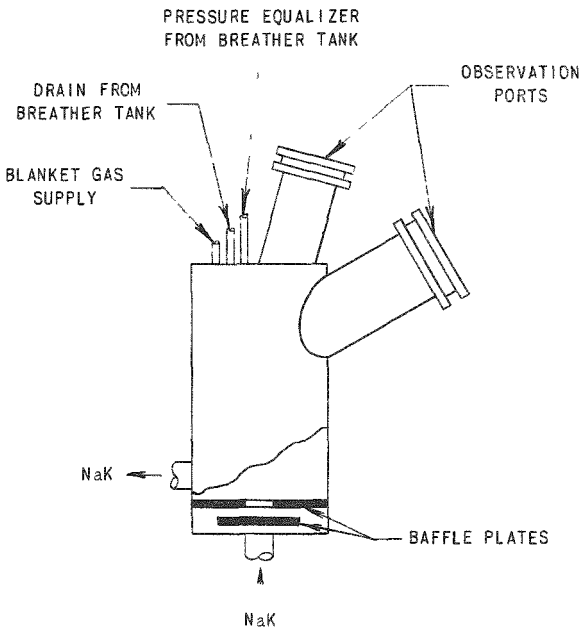

Fig. 9. Expansion Tank

Three $\frac{1}{4}$-in. pipe lines entered the top of the tank: (1) a line to the system blanket gas supply; (2) a drain line from the breather tank; (3) a pressure-equalizing line to the breather tank. It should be noted that any gas not removed by the separator could have been removed in the expansion tank, where it would be passed through the equalizing line to the breather tank.

C. Test Section

Figure 10 shows schematically the test section, which consisted of a long, rectangular channel of constant area with sudden contraction and expansion transitions to the 2-in. pipe. The channel was fabricated from 0.037-in. stainless steel with inside dimensions of $\frac{1}{4}$ in. by 2 $\frac{1}{32}$ in. The section was designed with a long, constant-area entrance length to allow the flow to develop as much as possible before reaching the magnetic field.

Points 1, 2, and 3 along the channel indicate the positions of pressure taps relative to the magnetic field. Measurements of void fraction were taken between tap 3 and the top of the magnetic field poles and between tap 1 and the bottom of the field poles, as indicated in Fig. 10. Pressure taps 1 and 3 were located 2 in. upstream and downstream, respectively, of the field poles so as to measure the total effect of the magnetic field and to allow for the apparatus for void measurement.

D. Accessories and Instrumentation for Test Section

1. Pressure and Pressure Drop

Pressure drops in the test section were determined with either a ±1- or a ±15-psid Statham transducer, depending on test conditions. The transducers were initially calibrated against a water and a mercury manometer, respectively. Transducer output was read on a Brown recorder.

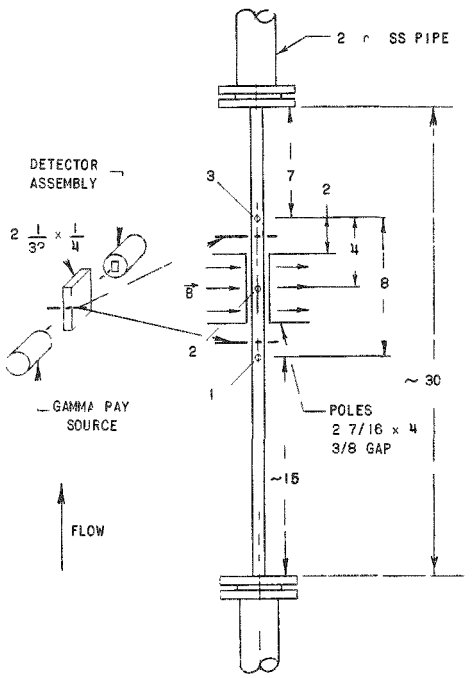

Fig. 10. Test Section (dimensions in in.)

Pressure was measured at tap 1, that is, upstream of the magnetic field, by opening one side of the transducer to the atmosphere. The pressure at tap 3, that is, downstream of the field, was then determined by subtracting the pressure drop between the two points.

Because of the difficulties involved in handling NaK, the system of pots shown in Fig. 11 was devised. NaK was bled from the pressure taps into the pots, which contained kerosene. When the system was in operation, pressure was transmitted through the NaK-kerosene interfaces in the pots to the transducer.

The pots were constructed from 2-in. Pyrex pipe fittings, the ends of which were blanked off with stainless steel plates and sealed with Buna N O-rings. One-quarter-inch stainless steel tubing was used between the pressure taps and the pots, and between the pots and transducer. Needle valves with asbestos-graphite packing were used in the NaK lines. The kerosene lines were controlled with Teflon-packed valves.

2. Void Fraction

A gamma-ray attenuation technique was used in the determination of void fraction. Initially, measurements were made via the "one-shot" technique[4] to obtain a rough idea of the effect of the magnetic field. Later, a more accurate traversing technique[3] was employed.

3. Magnetic Field

Power for the DC electromagnet used in this study was obtained from a 3-phase, 440-V, Ther Rectifier with a maximum output of 3000 A at 2 V. Current output was controlled with a "stepper-switch" on the power supply. This resulted in current available at

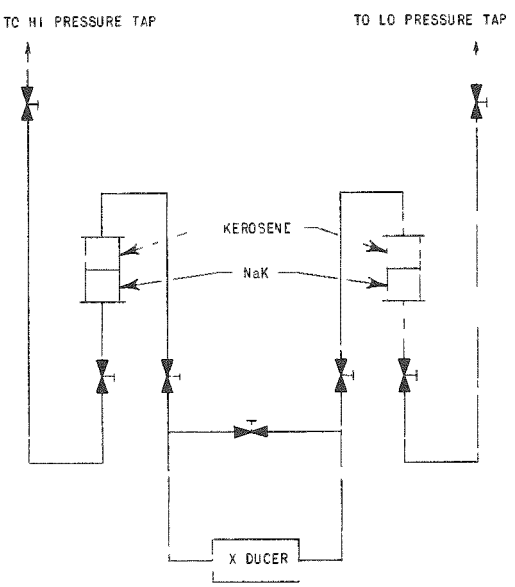

Fig. 11. System for Measuring Pressure Drop in Test Section

certain discrete values which could be obtained consistently and which remained relatively constant during each run. Current output was determined by measuring the potential drop across a known shunt resistance with a recording potentiometer. This also provided a record of current consistency during each run.

The magnet itself was series wound with windings consisting of $\frac{1}{4}$-in. by 4-in. copper bus bar. Connections with the power supply were also made with $\frac{1}{4}$-in. by 4-in. copper bus bar. Pole faces were $2\frac{7}{16}$ in. by 4 in. with a $\frac{3}{8}$-in. gap.

Before the test section was placed in the loop, a curve of average magnetic field strength vs current input was determined with a Radio Frequency Laboratories Model 1295 Gaussmeter. The Gaussmeter was a direct-reading transistorized instrument operating on the Hall effect principle and had a range of 50 kG. The probe used in the determination of field strength was initially calibrated against a 1000-G Alnico V Reference Magnet. The field strength was recorded at 24 points distributed over the area of the pole face and midway between the poles. The field was found to be uniform within 5% across the pole. This is well within the accuracy of the determination because of the criticality of the angle of the face of the probe with respect to the pole face. Fringing effects could not be determined accurately because of the finite size of the probe. Indications were, however, that the field strength fell off very rapidly past the edges of the pole faces. The assumption of a uniform field with abrupt edges was, therefore, reasonably justified.

III. DISCUSSION OF RESULTS

A. Single-phase Results

Single-phase data were procured as part of this investigation to provide information which, when compared with present or future developments in single-phase theory, would serve as a starting point for the theoretical understanding of the two-phase problem.

Figure 12 is representative of the experimental and calculated[4] total pressure drops obtained for single-phase flow without a magnetic field. Even though the three sets of data shown in Fig. 12 were not obtained simultaneously, the experimental pressure drop between taps 1 and 2 was essentially equal to that between taps 2 and 3, and the sum of these two pressure drops approximately equaled the value measured between taps 1 and 3. This correlation, together with the close agreement between the calculated and experimental results, indicated that the test section and pressure taps were probably free of geometric imperfections and that the instrumentation was operating properly.

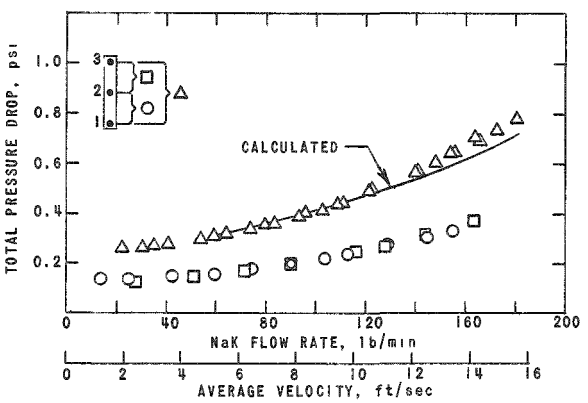

Fig. 12. Total Pressure Drop vs NaK Flow Rate; Single-phase, 0 Gauss

Figures 13 through 17 present data for pressure drop versus average velocity at various magnetic field strengths. The term "magnetic pressure drop" refers to the total pressure drop between taps minus the appropriate head or potential loss between the two points.

Comparison of these figures with Fig. 12[5] reveals the difference between the small frictional pressure drop when the field is not present and the large frictional and induction drag pressure drop when the field is present. This effect is also indicated by the value of the Hartmann number M, a ratio of the magnetic "viscous" force per unit volume to the ordinary viscous force per unit volume:

---

[4]The hydraulic similarity between NaK and more familiar fluids makes possible the direct application of the usual methods of calculating single-phase pressure drop.(8)

[5]Figure 12 is presented with <u>total</u> pressure drop as ordinate. The above comparison should be made with total pressure drop minus head or potential loss where the latter is indicated on Fig. 12 by the intersection of the curves with the line: average velocity = 0.

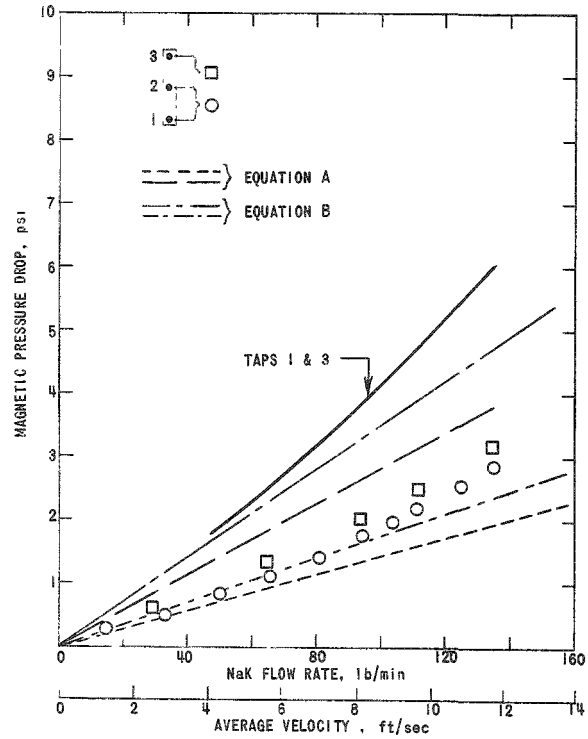

Fig. 13. Magnetic Pressure Drop vs NaK Flow Rate; Single-phase, 4300 Gauss; M = 82

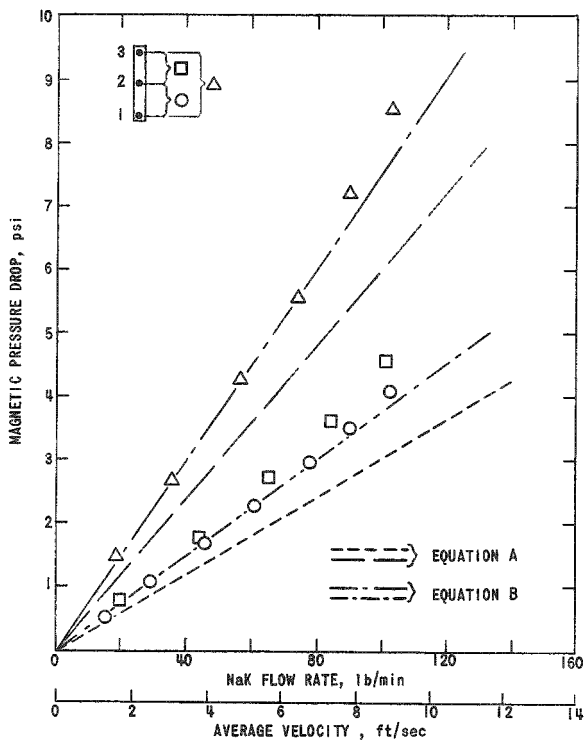

Fig. 14. Magnetic Pressure Drop vs NaK Flow Rate; Single-phase, 6370 Gauss; M = 122

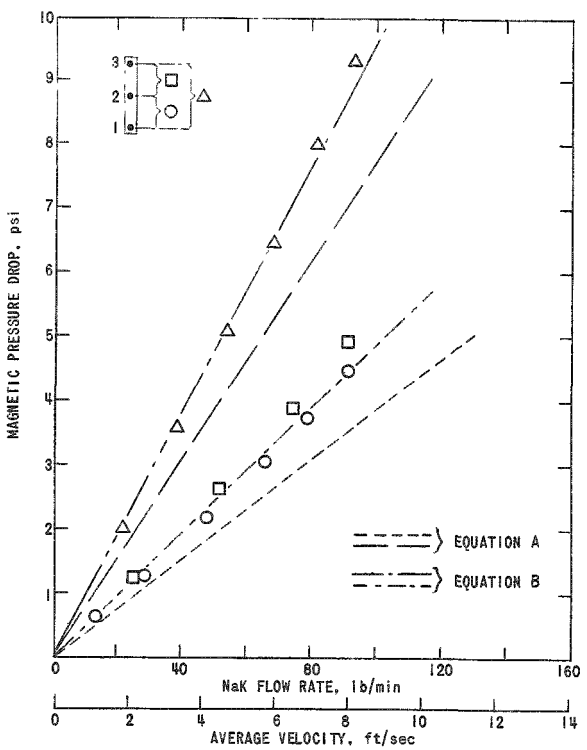

Fig. 15. Magnetic Pressure Drop vs NaK Flow Rate; Single-phase, 7280 Gauss; M = 139

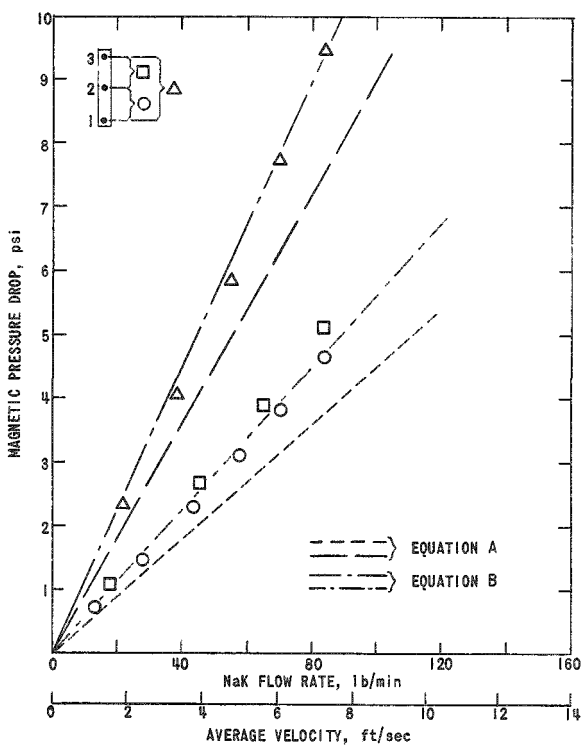

Fig. 16. Magnetic Pressure Drop vs NaK Flow Rate; Single-phase, 7840 Gauss; M = 150

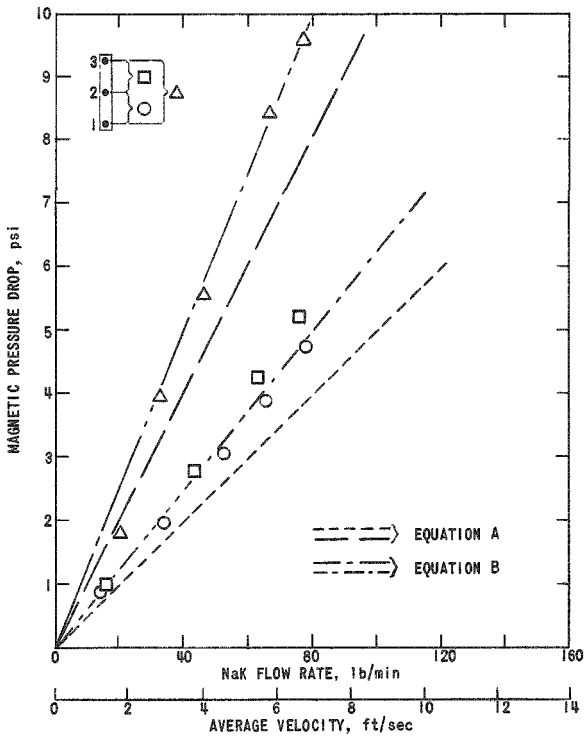

Fig. 17

Magnetic Pressure Drop vs NaK Flow Rate; Single-phase, 8270 Gauss; M = 158

$$M = B_0 a(\sigma/\eta)^{1/2},$$

where

B_0 = magnetic field strength, Webers/m^2;

a = half-width of channel in field direction, m;

σ = electrical conductivity of fluid, mho/m;

η = viscosity, kg/m-sec.

Values of M ranged from 82 to 158 in this phase of the investigation.

At all times that an applied magnetic field was present, the pressure drop between taps 1 and 2 was less than that between 2 and 3, even though the sum of these two was approximately equal to the measured value between 1 and 3.[6] This difference was probably due to the difference in edge effect when entering and leaving the imposed field region.

The "edge effect" initially arises because the magnetic field must fall off in the flow direction at the entrance and exit to the field region.

---

[6]In Fig. 13, a line indicates the sum of the pressure drops between taps 1 and 2, and 2 and 3, since data for taps 1 and 3 were not obtained at 4300 Gauss.

When a fluid flows through these "edges," induced currents circulate in planes parallel to the flow direction and perpendicular to the imposed field direction. The "end" currents then give rise to induced magnetic fields which oppose the applied magnetic field at the entrance to the imposed field region and reinforce the applied field at the exit. The resulting distortion of the applied field may lead to a difference in pressure drop on entering and leaving the imposed field region.

Curves designated as equation "A" represent pressure drops calculated from the following equation, which is developed in Appendix A according to derivations given by Shercliff[1] and Jackson:[2]

$$p_0 = L\sigma B_0^2 V_0 \left[\frac{1}{M} + \frac{d}{1+d}\right], \qquad (A)$$

where

p_0 = pressure drop due to uniform magnetic field of length L;

V_0 = average velocity;

$d = w\sigma_w/a\sigma$ = wall conductivity number;

w = thickness of channel wall perpendicular to B_0;

σ_w = conductivity of wall.

In the derivation of the equation the flow of an electrically conducting, viscous, incompressible fluid, with the permeability and permittivity of free space is assumed to be through a constant-area rectangular channel with a uniform, static, transverse magnetic field parallel to the short side of the channel cross section. The walls are assumed to be perfectly conducting parallel to the field and of finite conductivity perpendicular to the field. These conditions were approximated to a reasonable degree in the test facility with the possible exception of an unsettled velocity profile (especially at low strengths of the magnetic field).

The major portion of the difference between experimental data and the results predicted by the above equation was attributed to the aforementioned edge effects. Curves designated equation "B" represent pressure drops calculated by means of the following equation:

$$p_0' = L\sigma B_0^2 V_0 \left[\frac{1}{M} + \frac{d}{1+d}\right] + \sigma B_0^2 V_0 b (d')^{1/2}, \qquad (B)$$

where

p_0' = pressure drop due to uniform magnetic field of length L and due to edge effects;

b = half-width of channel cross section perpendicular to B_0 direction;

d' = wall conductivity number based on b.

The first part of equation (B) takes into account the effect of the uniform field. The second portion is given in Shercliff[1] as part of an approximate analysis to take into account end-current pressure losses.

The following are some of the assumptions underlying the analysis:[1]

1. There exist abrupt edges to the imposed magnetic field. This was believed to be reasonably approximated in the equipment.

2. The applied magnetic field is purely transverse and not seriously distorted by the flow. The approximation is questionable, especially under the test conditions where field distortion would be most severe, that is, at the relatively high flow rates which were attained under conditions of low magnetic field strength.

3. There exists a uniform velocity distribution in the region prior to the applied field. This was not the case since the long entrance length (approximately 30 equivalent diameters) before the field region would result in the development of a nonuniform velocity profile.

4. Circulation of end currents occurs only in planes perpendicular to the applied field. End-current loops were not restricted to planes perpendicular to the imposed field because of the nonuniform velocity profile and the conducting walls at $x = \pm a$ (see Fig. 37).

5. Either the wall conductivity is high or d' is so large that the axial part of the end currents flow almost entirely in the walls at $y = \pm b$ (see Fig. 37). In the test facility the major portion of the axial components of the end-current loops probably flowed in the fluid since d' was relatively low (~ 0.02).

6. There is no direct contact between walls ($y = \pm b$) at ends of the uniform field region. Direct contact in the form of walls at $x = \pm a$ (see Fig. 37) did exist. In this instance, Shercliffe[1] states that the end-current pressure losses, as given by the last part of equation "B," should be increased by a factor of two. However, this factor was neglected since the wall thickness was small compared with the dimension "A" of the fluid and since the conductivity of the wall material was about one-half that of

the NaK.[7] The effect of the "direct contact" in this case, was probably much less than the effect of neglecting a nonuniform velocity profile. Both conditions lead to distortions of the end-current loops such that they would no longer circulate in planes perpendicular to the imposed field. The result is an expansion of the original two-dimensional problem to an untractable problem in three dimensions.

In spite of the apparent differences between the assumptions of the analysis and the characteristics of the test facility, an agreement between the calculated and experimental pressure drop was obtained.

Examination of Figs. 13 through 17 indicates the best agreement between the calculated and measured pressure drop occurred for the higher values of magnetic field strength. It is reasonable to assume that, for a given average velocity, the time needed to develop fully the flow in the presence of a field would decrease as the strength of that field increased. Therefore, the calculation, which is based on developed flow, would tend to deviate less for a given flow rate as field strength increased.

Equation "B" states that total magnetic pressure drop for a given test facility and a constant average velocity is a function of B_0^2. However, as the plots of experimental data in Fig. 18 indicate, the exponent of B_0 should not be 2, but considerably less. If the flow is assumed to be developed in the field region (which is probably true under conditions of high field strength), then the first part of equation "B" holds. The data indicate that, under these test conditions, the end-current pressure losses are a function of B_0 with an exponent less than 2.

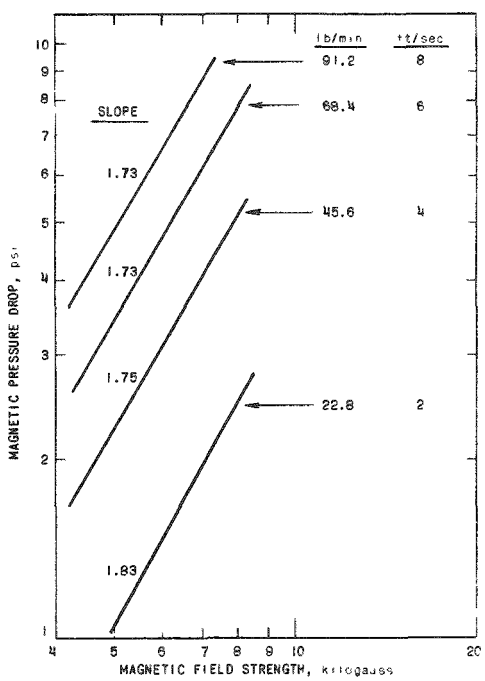

Fig. 18

Log (Magnetic Pressure Drop) vs Log (Magnetic Field Strength); Single-phase Cross Plot

[7] $\sigma_{wall} \approx 1.4 \times 10^6$ mho/m; $\sigma_{NaK} \approx 2.4 \times 10^6$ mho/m.

B. Two-phase Flow

1. Void Distribution

Examples of void distributions obtained before and after the magnetic field region (see Fig. 10) are shown in Figs. 19 through 22. All distributions were taken across the narrow part of the channel, that is, they represent void profiles in a plane parallel to the direction of flow and to the direction of the applied magnetic field.

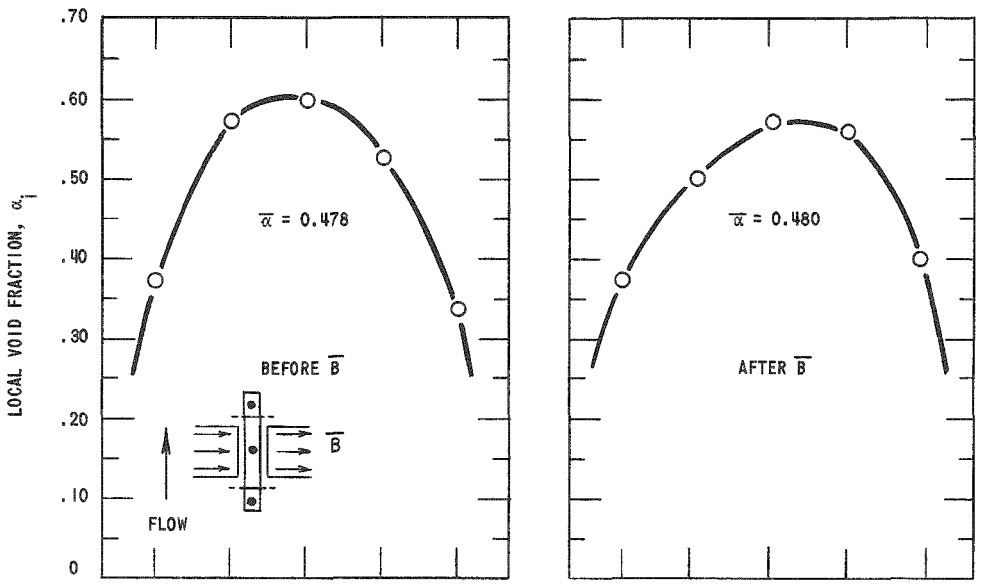

Fig. 19. Distribution of Voids before and after Field; 0 Gauss, NaK Flow = 14.5 lb/min

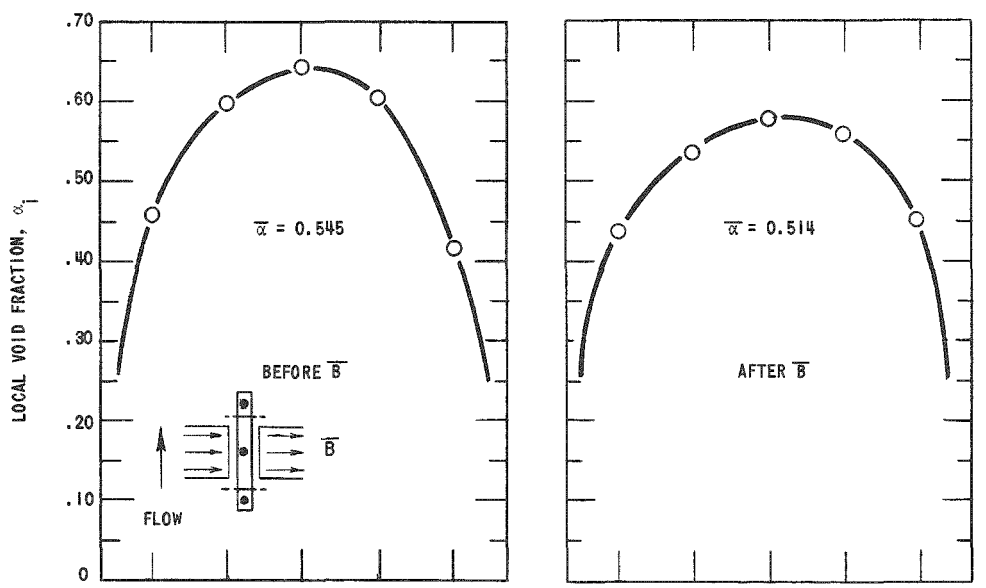

Fig. 20. Distribution of Voids before and after Field; 4300 Gauss, NaK Flow = 14.5 lb/min

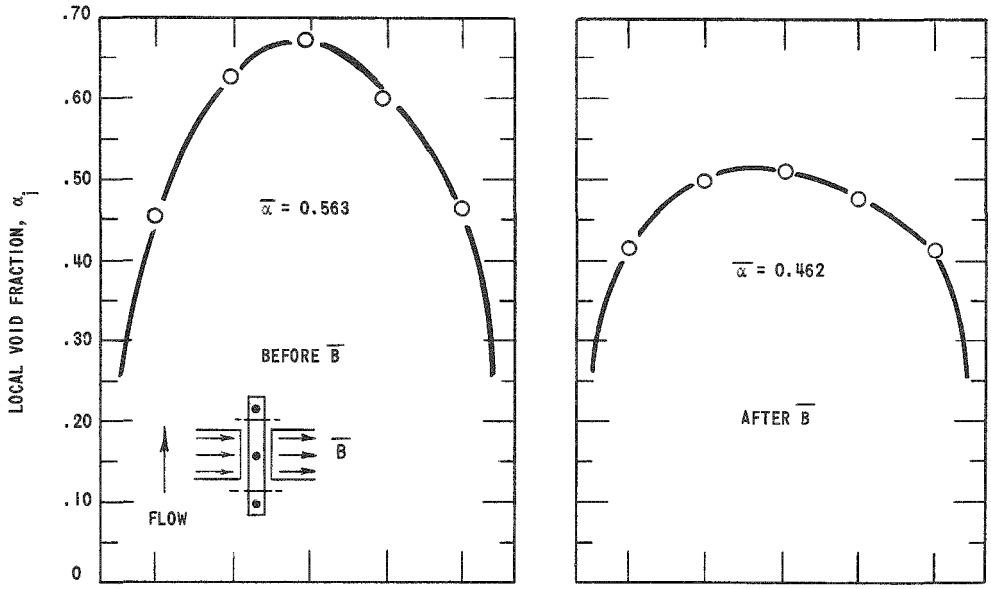

Fig. 21. Distribution of Voids before and after Field; 7840 Gauss, NaK Flow = 14.5 lb/min

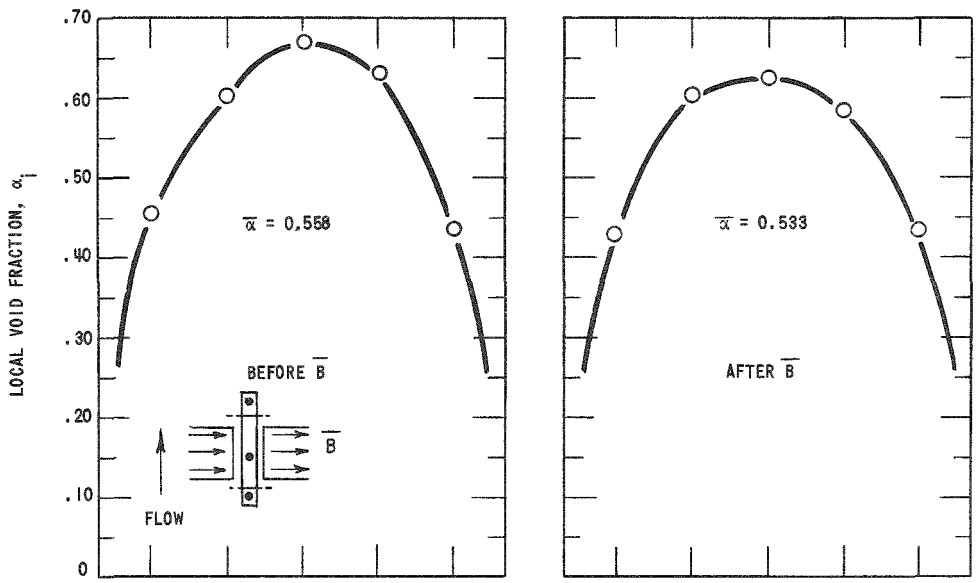

Fig. 22. Distribution of Voids before and after Field; 7840 Gauss, NaK Flow = 50 lb/min

Figure 19 shows that, under the condition of zero field, the profiles at the two traversing positions are similar and parabolic, and have very nearly the same value for average cross-sectional void fraction, $\overline{\alpha}$ (i.e., the ratio of the area occupied by the gas phase to the total flow area at a given cross section). This indicates that the flow was reasonably settled and not under the influence of unusual hydrodynamic forces.

Comparison of Figs. 20 and 21 with Fig. 19 shows that applying a magnetic field and increasing the field strength under conditions of constant flow rate of NaK and approximately constant average void fractions upstream of the field led to a flattening of the void profile. The effect was more pronounced with increased field strength.

The effect of an increased NaK flow rate under a condition of constant field strength and approximately constant upstream average void fraction is shown by comparison of Figs. 21 and 22. Increase of the NaK flow rate decreased the flattening effect on the profile and, in turn, led to a smaller change in average void fraction.

The decrease in average void fraction corresponding to the flattening of the void profile was probably due to the strong interaction of the field with the mixture in terms of a decrease in the velocity of the liquid.[8] This, in turn, would decrease the area available to the gas. The overall effects of the magnetic field are better discussed in terms of changes in slip ratio and in pressure drop, and will be discussed in the next sections.

In this investigation there was no observable tendency for the magnetic field to shift the voids to either side of the channel, that is, in the direction of the imposed field. Void distributions in a plane parallel to the flow and perpendicular to the applied field could not be determined with the apparatus.

2. Slip Ratio

Figure 23 illustrates the observed effect of the magnetic field on the average void fraction before and after the imposed field as the nitrogen

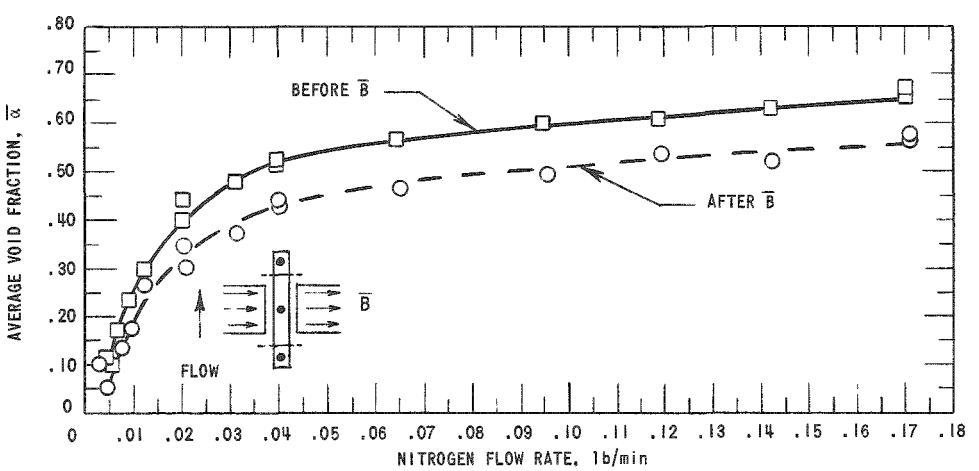

Fig. 23. Average Void Fraction before and after Field vs Nitrogen Flow Rate; 7840 Gauss, NaK Flow = 14.5 lb/min

[8]The electromagnetic forces would not act directly on the gas phase because of the negligible conductivity of that phase.

flow rate varies and the NaK flow rate is held constant. Plots of this type under no field conditions yielded, essentially, a single curve, since changes in void fraction between the two positions was negligible.

For a given NaK flow rate the difference between the curves increased with increased magnetic field strength. This was probably due to the increase in interaction between the field and the mixture with the corresponding increase in holdup of the liquid.

For a given field strength, an increase in NaK flow rate leads to a smaller difference between curves as plotted in Fig. 23, even though the increase in average liquid velocity would seem to indicate a stronger interaction with the field. This, together with the effects of field-strength variation mentioned above, is best studied in terms of the ratio of the average velocity of the gas phase at a given cross section to the average velocity of the liquid phase at that cross section. This "slip ratio" was calculated from the following equation for positions before and after the imposed field:

$$\frac{V_g}{V_\ell} = \frac{\dot{m}_g}{\dot{m}_\ell} \frac{(1-\bar{\alpha})}{\bar{\alpha}} \frac{\rho_\ell}{\rho_g} ,$$

where

V_g = average velocity of the gas phase at a given cross section;

V_ℓ = average velocity of the liquid phase at the same cross section;

$\dot{m}_g$ = mass rate of flow of gas;

$\dot{m}_\ell$ = mass rate of flow of liquid;

$\bar{\alpha}$ = average void fraction at the cross section;

ρ_ℓ = density of liquid;

ρ_g = density of gas.

This expression may be derived from the steady-state incompressible continuity equation by applying the equation first to the gas phase at a given cross section, then to the liquid phase at the same cross section, and taking a ratio of the two. This must be done in view of the fact that the flow areas available for gas and liquid flow at a given cross section are $\bar{\alpha}A$ and $(1-\bar{\alpha})A$, respectively, where A is the total cross-sectional area.

Figures 24 through 29 show such slip ratios before and after the field as a function of nitrogen flow rate under conditions of constant NaK flow rate and constant magnetic field strength.

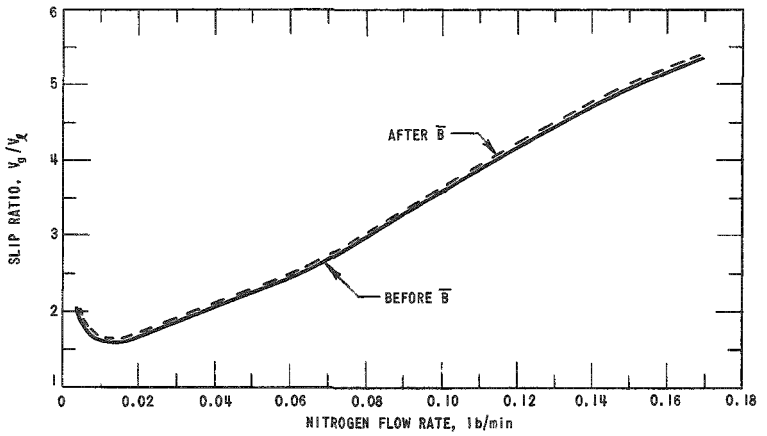

Fig. 24. Slip Ratio before and after Field vs Nitrogen Flow Rate; 0 Gauss, NaK Flow = 14.5 lb/min

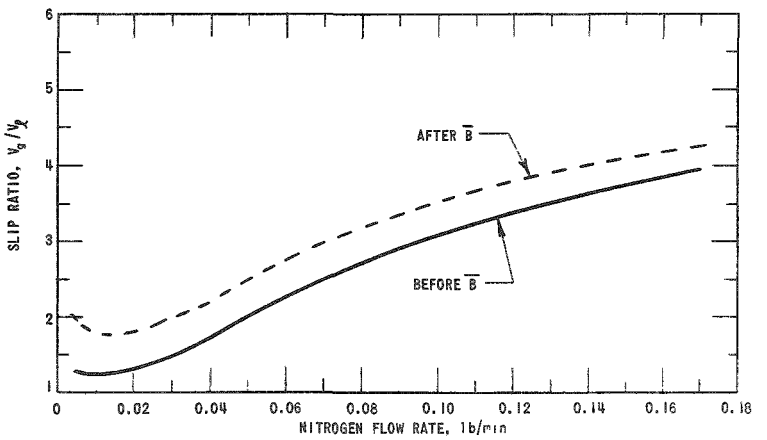

Fig. 25. Slip Ratio before and after Field vs Nitrogen Flow Rate; 4300 Gauss, NaK Flow = 14.5 lb/min

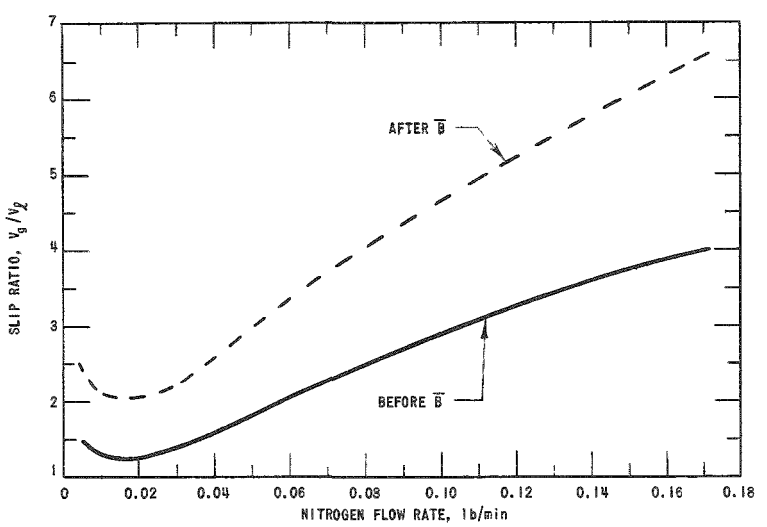

Fig. 26. Slip Ratio before and after Field vs Nitrogen Flow Rate; 7840 Gauss, NaK Flow = 14.5 lb/min

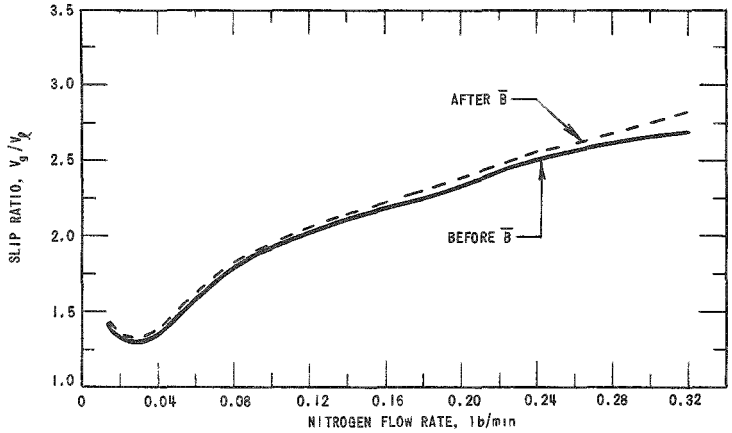

Fig. 27. Slip Ratio before and after Field vs Nitrogen Flow Rate; 0 Gauss, NaK Flow = 50 lb/min

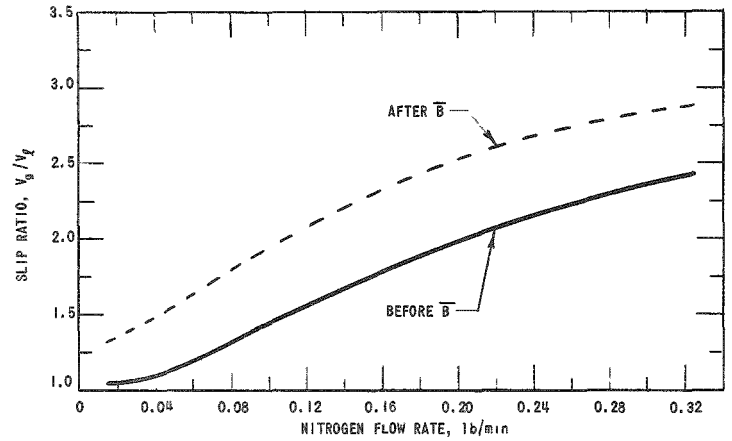

Fig. 28. Slip Ratio before and after Field vs Nitrogen Flow Rate, 4300 Gauss, NaK Flow = 50 lb/min

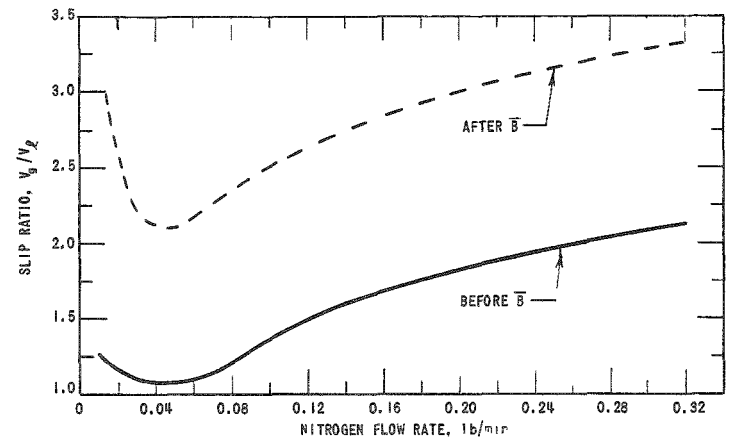

Fig. 29. Slip Ratio before and after Field vs Nitrogen Flow Rate; 7840 Gauss, NaK Flow = 50 lb/min

The very small difference between the curves under no-field conditions, shown in Figs. 24 and 27, may be attributed to the negligible change in void fraction and the very small pressure drop under these conditions. The difference in slip ratio for each of these cases was due only to the small change in the density of the gas, since all other factors were constant in the above equation. Comparison of Figs. 24 through 29 indicates the large effect of applying and increasing the strength of the magnetic field.

Figure 30 is a plot of change in slip ratio (V_g/V_ℓ after the field, minus V_g/V_ℓ before the field) as a function of the average void fraction over the flow length in the field region, $\overline{\overline{\alpha}}$. Here $\overline{\overline{\alpha}}$ is defined as the arithmetic mean of the average void fraction at cross sections before and after the field:

$$\overline{\overline{\alpha}} = \frac{1}{2}(\overline{\alpha}_b + \overline{\alpha}_a),$$

where $\overline{\alpha}_a$ and $\overline{\alpha}_b$ are the average void fractions at cross sections before and after the field region. It has been assumed that the effect of the field on the void fraction is linear in the flow direction, which is probably a reasonable first approximation.

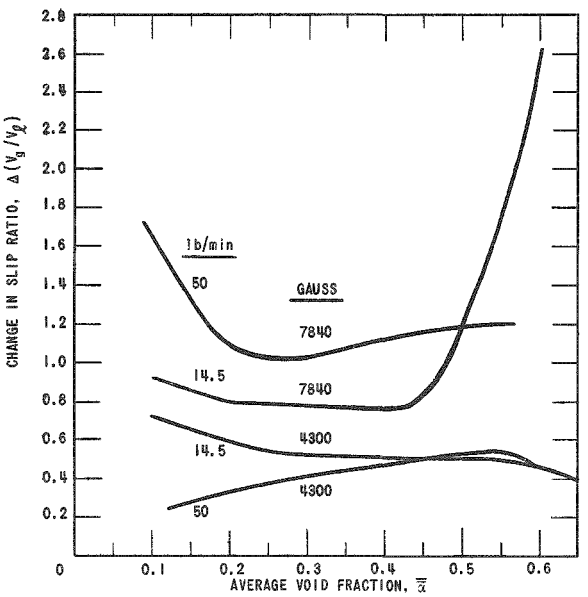

Fig. 30. Change in Slip Ratio vs Average Void Fraction in Flow Direction

Even though the locations for the determination of flow characteristics (see Fig. 10) were a finite distance away from the field region, changes in flow phenomena when a field was present were attributed solely to that field, that is, the small changes due to the usual hydrodynamic forces in the regions between the area of field interaction and the measurement locations were neglected. This was reasonable since the effect would be even less than the very small changes which were determined without a magnetic field.

The curves in Fig. 30 represent conditions of constant NaK flow rate and constant applied magnetic field strength as indicated. The very small change in slip ratio which occurred without a magnetic field (see Figs. 24 and 27) would appear as curves very nearly coincident with the horizontal axis in Fig. 30 and are, therefore, not shown. In all cases, the indicated changes in slip ratio at low values of void fraction are probably in error for reasons stated earlier and will not be discussed.

All four curves in Fig. 30 are relatively constant over a large portion of the range of $\bar{\bar{\alpha}}$ under consideration. This indicates that the electromagnetic forces acting on the mixture were also approximately constant over this range of $\bar{\bar{\alpha}}$, for conditions of constant NaK flow rate and given magnetic field strength. If it is assumed that, under these conditions, the net electromagnetic force on the mixture is a function only of the average liquid velocity and of the conductivity of the mixture, the effect can be attributed to a balancing between the increased liquid velocity and decreased conductivity associated with an increased average cross-sectional void fraction.

The difference in level between the relatively constant portions of the curves at a magnetic field strength at 7840 G indicates that a greater force acts on the mixture for the higher NaK flow rate. This was probably due to the corresponding higher average liquid velocity. The sudden upturn in the curve for low flow rate may have resulted from a change in flow regime, that is, from a highly turbulent flow pattern with the gas phase dispersed in the liquid phase to a slug or annular flow in which most of the liquid is located around the periphery of the channel and most of the gas in a central core. This was evidenced by a sudden increase in pressure-drop fluctuations, a characteristic usually associated with this change in flow regime. With the new flow pattern the field may have been better able to "holdup" the liquid phase, resulting in a greater change in slip ratio and the corresponding sudden upturn in the curve. At the higher flow rate of liquid, the sudden change in pressure-drop fluctuation was not noted. This indicated that a change in flow regime probably did not occur and may be an insight as to why the curve for the higher flow rate shows no indication of the sharp upturn present in the curve for the low flow rate with the same value of field strength.

Decreasing the magnetic field strength decreases the forces on the fluid and yields the smaller changes in slip ratio as shown in the two lower curves of Fig. 30. At this lower value of field strength, 4300 G, electromagnetic forces were probably not strong enough to result in a significant difference between the relatively constant values for change in slip ratio for the two NaK flow rates under consideration. It is also reasonable to assume that the holdup forces on the liquid were probably not sufficient to result in a change in flow regime under these conditions and, therefore, the curves show no sudden upturn.

3. Pressure Drop

Figures 31 and 32 are examples of the measured total pressure drops between taps 1 and 2, 2 and 3, and 1 and 3 under conditions of constant NaK flow rate and variable gas flow rate with and without an applied magnetic field. The relatively constant value of total pressure drop with increasing gas flow rate was a result of a decreasing head or potential

loss, a small change in momentum, and an increasing frictional and/or magnetic loss. As in the case of the single phase considered earlier, magnetic pressure loss refers to the large additional losses which occur when the field is applied.

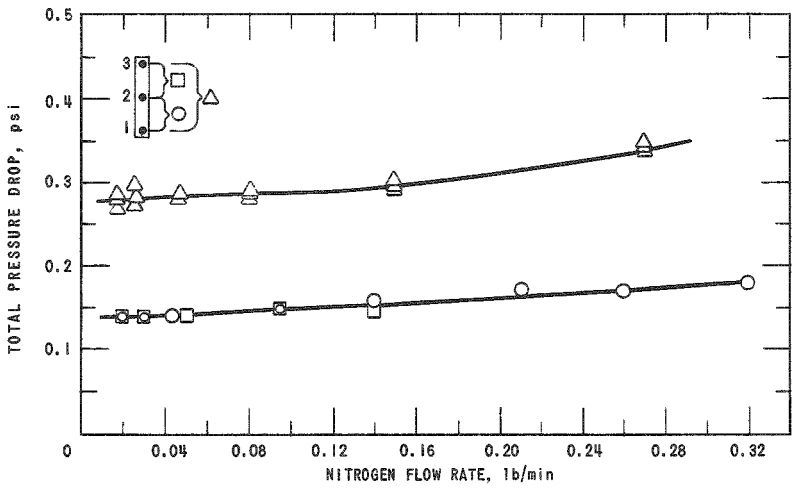

Fig. 31. Total Pressure Drop vs Nitrogen Flow Rate; 0 Gauss, NaK Flow Rate = 50 lb/min

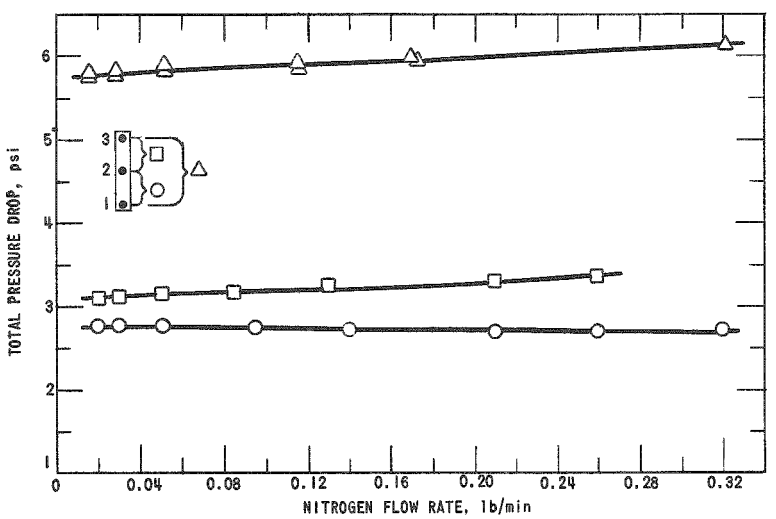

Fig. 32. Total Pressure Drop vs Nitrogen Flow Rate; 7840 Gauss, NaK Flow Rate = 50 lb/min

The difference in pressure drops between taps 1 and 2 and taps 2 and 3 in Fig. 32 was probably due to edge effects. However, in the discussion which follows edge effects are neglected as a first approximation, and the pressure drop between taps 1 and 3 is attributed to a uniform magnetic field.

Figures 33 and 34 show the relation between the magnetic pressure drop and $\overline{\overline{\alpha}}$ (as defined earlier) for the constant values of NaK flow rate and magnetic field strength indicated. Magnetic pressure drop was determined from the total pressure drop measured between taps 1 and 3 by subtracting head or potential loss (based on $\overline{\overline{\alpha}}$) and correcting for any change in the momentum of the liquid arising from a change in $\overline{\alpha}$. Momentum changes arising from the gas phase were neglected. The large magnitude of the pressure drop due to the field is brought out by comparison with the bottom curves in Figs. 33 and 34, which represent the relatively small frictional losses without the field.

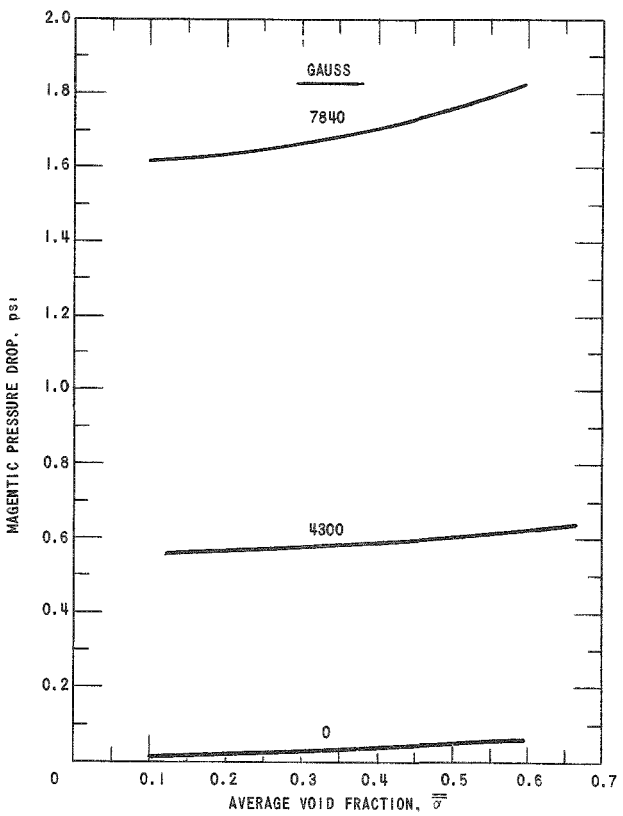

Fig. 33. Magnetic Pressure Drop vs Average Void Fraction; NaK Flow Rate = 14.5 lb/min

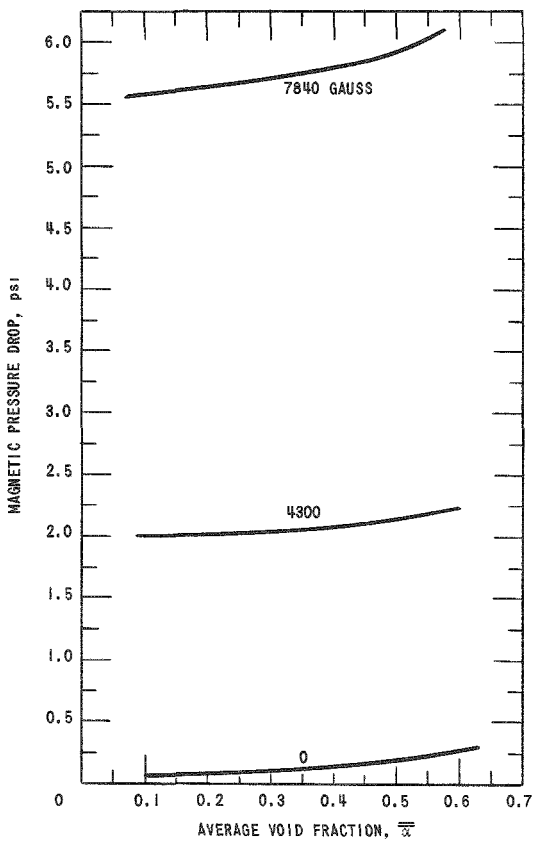

Fig. 34. Magnetic Pressure Drop vs Average Void Fraction; NaK Flow Rate = 50 lb/min

If the assumption is again made that the electromagnetic forces on the mixture are dependent only on the liquid velocity and the conductivity of the mixture for a condition of constant field strength, then the relatively constant values of magnetic pressure drop may be attributed to the balancing effect of the increase in average liquid velocity and decrease in conductivity with increasing cross-sectional void fraction.

Figures 35 and 36 show the friction factor multiplier defined for a constant liquid flow rate as the two-phase pressure drop over a given flow

length divided by the liquid pressure drop over that same flow length. The large effect of the gas phase on the frictional pressure drop under normal flow conditions is exemplified by the large slope of the zero-field curves in the two graphs. A close comparison is shown with the work of Petrick[3] who presented the friction factor multiplier as a function of void fraction for air-water flow in a vertical $\frac{1}{4}$ x 2-in. channel.

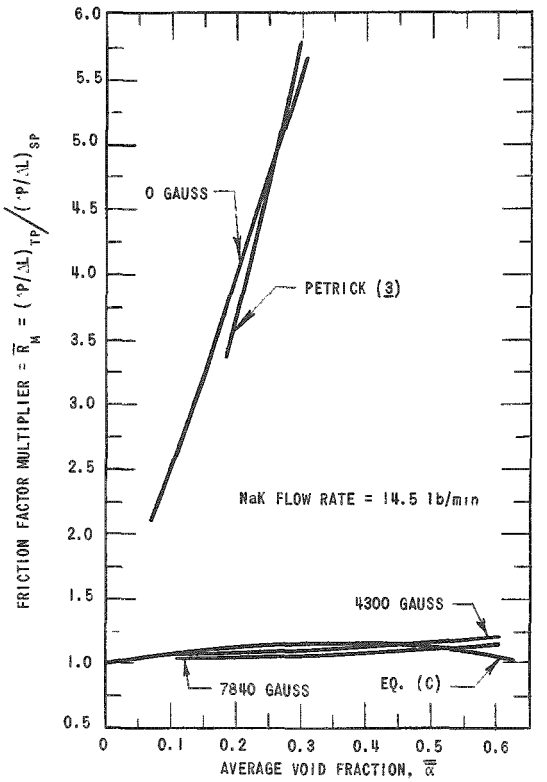

Fig. 35. Friction Factor Multiplier, $(\Delta P/\Delta L)_{TP}/(\Delta P/\Delta L)_{SP}$, vs Average Void Fraction; NaK Flow Rate = 14.5 lb/min

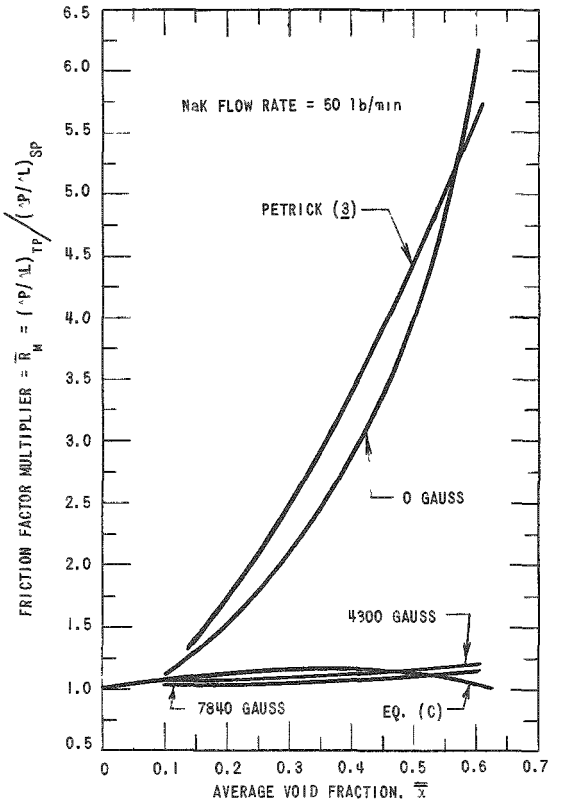

Fig. 36. Friction Factor Multiplier, $(\Delta P/\Delta L)_{TP}/(\Delta P/\Delta L)_{SP}$, vs Average Void Fraction; NaK Flow Rate = 50 lb/min

The relatively constant value of the magnetic friction factor multiplier, $\bar{R}_M$, representing the data taken in the presence of a magnetic field, indicates the small effect of the gaseous phase on the pressure drop under field conditions for this range of $\bar{\bar{\alpha}}$. Further increase in field strength would probably bring a curve of $\bar{R}_M$ closer to a constant value of one under these conditions. Curves designated as equation "C" represent a relation for magnetic friction factor multiplier developed in the following manner.

Equation "A" was rearranged to obtain the single-phase pressure gradient due to a uniform magnetic field:

$$\left(\frac{\Delta P}{\Delta L}\right)_{SP} = \sigma B_0^2 V_0 \left[\frac{1}{M} + \frac{d}{1+d}\right],$$

where ΔP is the pressure drop due to uniform magnetic field of length ΔL. It was assumed that the two-phase pressure drop was also a result of a uniform magnetic field of the same length and that the electromagnetic forces on the two-phase mixture under conditions of constant liquid flow rate and field strength were dependent only on the average liquid velocity and on the conductivity of the mixture. These were assumed to vary as follows:

$$V = \frac{V_0}{1 - \bar{\bar{\alpha}}}; \qquad \sigma_{TP} = \sigma \frac{(1 - \bar{\bar{\alpha}})^3}{1 - (\bar{\bar{\alpha}})^2},$$

where:

V_0 = average liquid velocity when void fraction is zero;

V = average liquid velocity when void fraction is $\bar{\bar{\alpha}}$;

σ_{TP} = electrical conductivity of two-phase mixture;

σ = electrical conductivity of liquid.

The expression for variation of conductivity with void fraction was developed by Petrick.[10]

Substitution of the above in equation "A" yields the following, where the subscript TP indicates the two-phase condition:

$$\left(\frac{\Delta P}{\Delta L}\right)_{TP} = \sigma \frac{(1 - \bar{\bar{\alpha}})^3}{1 - (\bar{\bar{\alpha}})^2} B_0^2 \frac{V_0}{(1 - \bar{\bar{\alpha}})} \left[\frac{1}{M_{TP}} + \frac{d_{TP}}{1 + d_{TP}}\right],$$

where

$$M_{TP} = B_0 a \left(\frac{\sigma}{\eta}\right)^{1/2} (1 - \bar{\bar{\alpha}})^{3/2} \left[1 - (\bar{\bar{\alpha}})^2\right]^{-1/2} = M (1 - \bar{\bar{\alpha}})^{3/2} \left[1 - (\bar{\bar{\alpha}})^2\right]^{-1/2}$$

and

$$d_{TP} = d \left[1 - (\bar{\bar{\alpha}})^2\right] (1 - \bar{\bar{\alpha}})^{-3}.$$

From the definition of $\bar{R}_M$:

$$\bar{R}_M = \left(\frac{\Delta P}{\Delta L}\right)_{TP} \Big/ \left(\frac{\Delta P}{\Delta L}\right)_{SP}$$

$$= (1 - \bar{\bar{\alpha}})^2 \left[1 - (\bar{\bar{\alpha}})^2\right]^{-1} \left[\frac{1}{M_{TP}} + \frac{\left[1 - (\bar{\bar{\alpha}})^2\right] (1 - \bar{\bar{\alpha}})^{-3} d}{1 + \left[1 - (\bar{\bar{\alpha}})^2\right] (1 - \bar{\bar{\alpha}})^{-3} d}\right] \left[\frac{1}{M} + \frac{d}{1 + d}\right]^{-1},$$

we obtain for large M and for $\bar{\bar{\alpha}}$ in the range under consideration

$$R_M = \frac{(1+d)}{(1-\bar{\bar{\alpha}})} \left\{1 + \left[1 - (\bar{\bar{\alpha}})^2\right] (1-\bar{\bar{\alpha}})^{-3} d\right\}^{-1}. \qquad (C)$$

Curves designated equation "C" in Figs. 35 and 36 were obtained from the above relation, which is a reasonable approximation for the magnetic friction factor multiplier under these conditions, even though the deviation becomes larger as $\bar{\bar{\alpha}}$ increases.

C. Conclusions

1. The application of the magnetic field tended to make the gas distribution more uniform in the field direction. This effect became more pronounced with increased field strength for a given flow rate of NaK. There was no observable tendency for the field to cause a major shift of the gas to either side of the channel in the direction of the imposed field.

2. The effect of the magnetic field was to increase slip ratio in all cases. This was probably due to the large difference in conductivity between the two phases, which led to greater electromagnetic forces on the liquid and a correspondingly high retarding action.

3. The introduction of the gas had very little effect on pressure drop for a given magnetic field strength and NaK flow rate over the range of void fraction which was considered. By assuming a simplified model, this was attributed to a balancing effect between the increase in average liquid velocity and decrease in the conductivity of the mixture as void fraction increased. This effect was predicted reasonably well by a magnetic, two-phase, friction factor multiplier based on the simplified model.

APPENDIX A

Derivation of Pressure Drop in a Uniform Field Region

The following are the basic MHD equations for an electrically conducting, viscous, incompressible fluid with the permeability and permittivity of free space. Their development as given below may be found in Shercliff[1] and Jackson.[2]

(a) The equation of motion in a fixed Cartesian coordinate system for a homogeneous, isotropic, incompressible, Newtonian fluid with the addition of the electromagnetic body-force term and the neglect of the gravity-force term is

$$\rho\left[\frac{\partial \overline{V}}{\partial t} + (\overline{V} \cdot \nabla)\overline{V}\right] = -\nabla p + (\overline{J} \times \overline{B}) + \eta \nabla^2 \overline{V}. \tag{1}$$

(b) Maxwell's equations (neglecting displacement currents) are

$$\nabla \times \overline{E} = -\frac{\partial \overline{B}}{\partial t} \tag{2}$$

$$\nabla \times \overline{B} = \mu_0 \overline{J}; \tag{3}$$

and

$$\nabla \cdot \overline{B} = 0. \tag{4}$$

(c) Ohm's Law, with conductivity taken as a scalar, is

$$\overline{J} = \sigma[\overline{E} + (\overline{V} \times \overline{B})]. \tag{5}$$

(d) The continuity equation is

$$\nabla \cdot \overline{V} = 0. \tag{6}$$

From (3) and (5),

$$\nabla \times (\nabla \times \overline{B}) = \mu_0 \nabla \times \overline{J} = \mu_0 \sigma[(\nabla \times \overline{E}) + \nabla \times (\overline{V} \times \overline{B})].$$

By means of (2) and (4), and the vector identity

$$\nabla \times (\nabla \times \overline{B}) = \nabla (\nabla \cdot \overline{B}) - \nabla^2 \overline{B},$$

we obtain

$$-\nabla^2 \overline{B} = \mu_0 \sigma\left[-\frac{\partial \overline{B}}{\partial t} + \nabla \times (\overline{V} \times \overline{B})\right],$$

or

$$\frac{\partial \overline{B}}{\partial t} - \nabla \times (\overline{V} \times \overline{B}) = \lambda \nabla^2 \overline{B}, \tag{7}$$

where

$$\lambda = 1/\mu_0 \sigma$$

is the magnetic diffusivity.

In the classical Hartmann problem, the flow of a viscous, incompressible fluid between infinite parallel planes a distance 2a apart is considered. A uniform, static magnetic field is assumed to be directed perpendicularly to these planes (see Fig. 37). The infinite extent in the y and z directions indicates that the solution is dependent only on x.

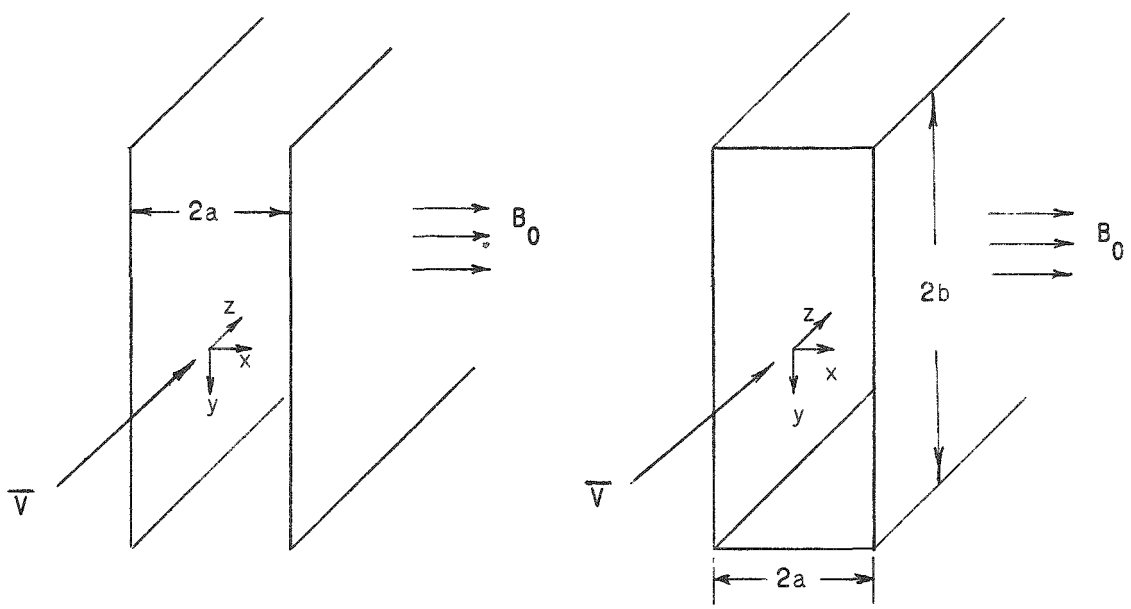

Fig. 37. Hartmann Problem

If the channel is now closed by two perfectly conducting plates in the xz plane, distance 2b apart, and it is assumed that the original velocity distribution is not disrupted, the situation is still one-dimensional and is usually referred to as Hartmann Flow. All current loops are assumed to lie in the xy plane, with the result that the induced magnetic field is in the z direction.

The following conditions describe the situation. Let $\overline{i}_x$, $\overline{i}_y$, and $\overline{i}_z$ be unit vectors in the coordinate system in Fig. 37. Then

$$\frac{\partial \overline{V}}{\partial t} = 0; \quad \frac{\partial \overline{B}}{\partial t} = 0; \tag{8}$$

$$\overline{V} = \overline{i}_z V_z(x); \tag{9}$$

$$\overline{B} = \overline{i}_x B_0 + \overline{i}_z B_z(x); \tag{10}$$

$$\overline{J} = \overline{i}_y J_y(x). \tag{11}$$

By the use of (8), (9), and (10) in (7), we obtain

$$\frac{\partial^2 B_z(x)}{\partial x^2} + \frac{B_0}{\lambda} \frac{\partial V_z(x)}{\partial x} = 0. \tag{12}$$

By the use of (8), (9), (10), and (3) in (1), we find

$$\frac{\partial p}{\partial x} = - \frac{B_z(x)}{\mu_0} \frac{\partial B_z(x)}{\partial x} \tag{13}$$

and

$$\frac{\partial p}{\partial z} = \frac{B_0}{\mu_0} \frac{\partial B_z(x)}{\partial x} + \eta \frac{\partial^2 V_z(x)}{\partial x^2}. \tag{14}$$

The total current per unit width in the y direction within the fluid may be obtained by integration of (5) [note that E_y = constant since $\overline{J} = \overline{i}_y J_y(x)$]:

$$I_f = \int_{-a}^{a} \sigma(E_y + VB_0)dx = 2a\sigma E_y + \sigma B_0 \int_{-a}^{a} V \, dx.$$

If we now define the mean fluid velocity V_0 by

$$V_0 = \frac{1}{2a} \int_{-a}^{a} V \, dx,$$

then

$$I_f = 2a\sigma(E_y + V_0 B_0).$$

If w and σ_w are, respectively, the thickness and conductivity of the channel walls perpendicular to B_0, then the current flowing in the wall per unit width in the y direction is given by

$$I_w = 2w\sigma_w E_y.$$

Since the net current in the y direction must be zero,

$$I_f + I_w = 2a\sigma(E_y + V_0B_0) + 2w\sigma_w E_y = 0$$

and

$$E_y = -\frac{V_0B_0}{\frac{w\sigma_w}{a\sigma} + 1} = \frac{V_0B_0}{d+1}, \tag{15}$$

where

$$d = w\sigma_w/a\sigma$$

is a measure of the effect of wall conductivity. By use of (5) and (3), and the condition that $\overline{V}$ must vanish at $x = \pm a$, we find

$$E_y = \frac{J_y(x)}{\sigma}\bigg|_{x=\pm a} = -\frac{1}{\mu_0\sigma}\frac{\partial B_z(x)}{\partial x}\bigg|_{x=\pm a} \tag{16}$$

which must also equal (15).

Integration of (12) and evaluation of the constant of integration via (15) and (16) yield

$$\frac{\partial B_z(x)}{\partial x} + \frac{B_0}{\lambda}V_z(x) - \frac{\mu_0\sigma V_0B_0}{1+d} = 0. \tag{17}$$

Upon substitution of (17) into (14) there is obtained

$$\frac{\partial^2 V_z(x)}{\partial x^2} - \frac{\sigma B_0^2}{\eta}V_z(x) = \frac{1}{\eta}\frac{\partial p}{\partial z} - \frac{\sigma B_0^2 V_0}{\eta(1+d)}. \tag{18}$$

Differentiation of (18) with respect to z gives

$$\frac{\partial^2 p}{\partial z^2} = 0.$$

Therefore,

$$\frac{\partial p}{\partial z} = \text{constant} = -\frac{p_0}{L}.$$

The general solution of (18) is

$$V_z(x) = C_1 \exp\left(M \frac{x}{a}\right) + C_2 \exp\left(-M \frac{x}{a}\right) + \frac{a^2}{M^2}\left[\frac{p_0}{\eta L} + \frac{M^2 V_0}{a^2(1+d)}\right], \qquad (19)$$

where

$$M^2 = B_0^2 a^2 \sigma/\eta = (\text{Hartmann number})^2.$$

By the use of (19) after finding C_1 and C_2, we find

$$V_0 = \frac{p_0 a^2(1+d)}{M^2 \eta L}\left[\frac{1 - \frac{\tanh M}{M}}{d + \frac{\tanh M}{M}}\right].$$

We then find the pressure drop due to the uniform magnetic field of length L to be

$$p_0 = \frac{L\eta V_0 M^2}{a^2(1+d)}\left[\frac{d + \frac{\tanh M}{M}}{1 - \frac{\tanh M}{M}}\right] = \frac{L\sigma B_0^2 V_0}{1+d}\left[\frac{d + \frac{\tanh M}{M}}{1 - \frac{\tanh M}{M}}\right]. \qquad (20)$$

As M becomes large, tanh $M \to 1$, and (20) becomes

$$p_0 = L\sigma B_0^2 V_0\left[\frac{1}{M} + \frac{d}{1+d}\right]. \qquad (21)$$

APPENDIX B

Tabulated Data

Table I

SINGLE-PHASE TOTAL* PRESSURE DROP VS NaK FLOW RATE

Magnetic Field, G	NaK Flow, lb/min	ΔP for Taps 1 and 3, psi	NaK Flow, lb/min	ΔP for Taps 1 and 2, psi	NaK Flow, lb/min	ΔP for Taps 2 and 3, psi	Magnetic Field, G	NaK Flow, lb/min	ΔP for Taps 1 and 3, psi	NaK Flow, lb/min	ΔP for Taps 1 and 2, psi	NaK Flow, lb/min	ΔP for Taps 2 and 3, psi
0	22	0.26	14	0.14	28	0.13	7280	22	2.25	14	0.76	26	1.38
	35	0.28	24	0.14	51	0.15		39	3.85	29	1.42	52	2.76
	59	0.31	42	0.15	72	0.17		54	5.35	48	2.31	75	4.02
	80	0.36	59	0.16	90	0.20		67	6.72	65	3.17	91	5.07
	96	0.41	75	0.18	116	0.25		81	8.25	79	3.87		
	108	0.45	90	0.20	127	0.27		92	9.58	91	4.60		
	122	0.50	103	0.22	144	0.32							
	140	0.57	113	0.24	163	0.37	7840	22	2.57	14	0.83	18	1.19
	154	0.64	128	0.27				39	4.32	28	1.58	46	2.78
	163	0.71	144	0.31				55	6.10	43	2.40	65	4.00
	180	0.78	155	0.33				70	7.95	58	3.21	84	5.24
								83	9.68	71	3.91		
4300			15	0.38	29	0.73				84	4.76		
			32	0.67	64	1.45							
			50	0.98	94	2.13	8270	21	2.03	15	0.98	16	1.14
			65	1.23	112	2.62		33	4.20	34	2.09	43	2.91
			81	1.54	135	3.27		46	5.80	52	3.18	63	4.38
			94	1.87				66	8.66	65	4.02	76	5.34
			103	2.13				76	9.90	78	4.87		
			111	2.30									
			125	2.65									
			135	2.95									
6370	18	1.75	15	0.67	20	0.91							
	36	2.95	29	1.19	44	1.90							
	57	4.55	46	1.81	65	2.80							
	75	6.02	61	2.38	85	3.70							
	90	7.47	78	3.08	102	4.69							
	103	8.79	90	3.63									
			102	4.22									

*Head or potential loss between taps 1 and 3 = 0.25 psi; head or potential loss between taps 1 and 2 = 0.125 ≈ 0.13 psi.

Table II

TWO-PHASE PRESSURE DROP; AVERAGE VOID FRACTION, $\bar{\alpha}$

$\dot{m}_g$, lb/min	Total Pressure Drop, psi			Pressure Tap 1, psi	$\bar{\alpha}$	
	Taps 1 and 3	Taps 1 and 2	Taps 2 and 3		Before $\bar{B}$	After $\bar{B}$
NaK Flow = 14.5 lb/min; 0 Gauss						
0.0038	0.24	0.13	-	-	-	-
0.0042	-	-	-	1.34	0.077	0.081
0.0073	0.22	0.11	-	-	-	-
0.0093	-	-	-	1.27	0.219	0.207
0.0120	0.22	0.11	-	-	-	-
0.0180	-	-	-	1.21	0.325	0.355
0.0201	0.19	0.10	0.10	-	-	-
0.0310	-	-	-	1.15	0.461	0.422
0.0385	0.18	-	-	-	-	-
0.0432	-	-	-	1.11	0.478	0.480
0.0500	-	0.09	0.08	-	-	-
0.0545	-	-	-	1.12	0.554	0.532
0.0642	0.17	-	-	-	-	-
0.0712	-	-	-	1.13	0.542	0.560
0.0950	-	0.09	0.08	-	-	-
0.1190	-	-	-	1.18	0.572	0.577
0.1400	-	-	0.08	-	-	-
0.1422	-	-	-	1.24	0.571	0.594
0.1700	0.16	0.08	-	1.31	0.594	0.616
NaK Flow = 14.5 lb/min; 4300 Gauss						
0.0038	-	0.40	-	-	-	-
0.0042	0.78	-	-	1.87	0.124	0.099
0.0073	-	0.39	-	-	-	-
0.0093	-	-	-	1.79	0.264	0.209
0.0120	-	0.39	-	-	-	-
0.0180	0.75	-	-	1.75	0.386	0.330
0.0200	-	0.38	0.40	-	-	-
0.0310	-	-	-	1.71	0.497	0.433
0.0432	0.73	-	-	1.67	0.540	0.484
0.0500	-	0.36	0.40	-	-	-
0.0545	-	-	-	1.73	0.545	0.514
0.0712	0.71	-	-	1.71	0.552	0.515
0.0950	-	0.35	0.40	-	-	-
0.1190	-	-	-	1.75	0.633	0.614
0.1400	-	-	0.42	-	-	-
0.1422	0.72	-	-	1.82	0.640	0.634
0.1700	0.72	0.34	-	1.89	0.652	0.659

Table II (Contd.)

$\dot{m}_g$, lb/min	Total Pressure Drop, psi			Pressure Tap 1, psi	$\bar{\alpha}$	
	Taps 1 and 3	Taps 1 and 2	Taps 2 and 3		Before $\overline{B}$	After $\overline{B}$
NaK Flow = 14.5 lb/min; 7840 Gauss						
0.0038	1.89	0.88	1.0	-	-	-
0.0042	-	-	-	2.95	0.108	0.056
0.0073	1.83	0.89	1.0	-	0.167	0.135
0.0093	-	-	-	2.94	0.231	0.175
0.0120	1.83	0.89	1.0	-	0.300	0.266
0.0200	-	0.90	0.98	-	-	-
0.0202	1.85	-	-	-	0.419	0.328
0.0310	-	-	-	2.89	0.478	0.371
0.0385	1.89	-	-	-	-	-
0.0395	-	-	-	-	0.520	0.434
0.0500	-	0.88	1.01	-	-	-
0.0642	1.87	-	-	-	0.563	0.462
0.0824	-	-	1.01	-	-	-
0.0950	-	0.87	-	2.90	0.599	0.492
0.1190	-	-	-	2.95	0.608	0.536
0.1422	-	-	-	3.00	0.629	0.521
0.1700	1.91	0.89	1.06	3.11	0.658	0.570
NaK Flow = 50 lb/min; 0 Gauss						
0.0172	0.279	-	-	-	-	-
0.0200	-	0.14	0.14	-	-	-
0.0262	0.280	-	-	-	-	-
0.0280	-	-	-	1.43	0.233	0.234
0.0295	-	0.14	0.14	-	-	-
0.0472	0.282	-	-	-	-	-
0.0492	-	-	-	-	0.304	0.295
0.0500	-	0.14	0.14	-	-	-
0.0512	-	-	-	1.44	0.329	0.325
0.0803	0.282	-	-	-	-	-
0.0950	-	0.15	0.15	-	-	-
0.1133	-	-	-	1.58	-	-
0.1308	-	-	-	-	0.473	0.447
0.1400	-	0.16	0.15	-	-	-
0.1501	0.296	-	-	-	-	-
0.1690	-	-	-	1.76	-	-
0.2100	-	0.17	-	-	0.535	0.542
0.2610	-	0.17	-	-	0.560	0.568
0.2730	0.339	-	-	-	-	-
0.3200	-	0.18	-	2.80	0.603	0.598

Table II (Contd.)

$\dot{m}_g$, lb/min	Total Pressure Drop, psi			Pressure Tap 1, psi	$\overline{\alpha}$	
	Taps 1 and 3	Taps 1 and 2	Taps 2 and 3		Before $\overline{B}$	After $\overline{B}$
NaK Flow = 50 lb/min; 4300 Gauss						
0.0155	2.21	-	-	3.22	0.149	0.145
0.0200	-	1.08	1.24	-	-	-
0.0295	2.19	1.05	1.24	3.18	0.278	0.210
0.0500	-	1.04	1.28	-	-	-
0.0503	2.20	-	-	3.14	0.349	0.312
0.0824	-	-	1.31	-	-	-
0.0937	2.21	-	-	3.22	0.459	0.415
0.0950	-	1.00	-	-	-	-
0.1210	2.20	-	-	3.26	0.485	0.442
0.1322	-	-	1.34	-	-	-
0.1400	-	0.99	-	-	-	-
0.2100	2.25	0.96	-	3.67	0.542	0.541
0.2600	-	0.96	-	-	-	-
0.2610	2.29	-	-	3.89	0.579	0.563
0.3200	2.31	0.99	-	4.25	0.604	0.596
NaK Flow = 50 lb/min; 7840 Gauss						
0.0155	5.78	-	-	6.97	0.120	0.057
0.0200	-	2.75	3.11	-	-	-
0.0280	5.79	-	-	6.97	0.209	0.160
0.0295	-	2.75	3.11	-	-	-
0.0500	-	2.76	3.13	-	-	-
0.0512	5.86	-	-	7.00	0.337	0.270
0.0824	-	-	3.19	-	-	-
0.0950	-	2.74	-	-	-	-
0.1133	5.88	-	-	7.28	0.437	0.365
0.1322	-	-	3.27	-	-	-
0.1400	-	2.73	-	-	-	-
0.1690	5.97	-	-	7.57	0.494	0.443
0.2100	-	2.72	3.30	-	0.524	0.485
0.2600	-	2.71	3.37	-	-	-
0.2610	-	-	-	-	0.558	0.533
0.3200	-	2.73	-	8.78	0.590	0.543
0.3220	6.13	-	-	-	-	-

Table III

VOID DISTRIBUTIONS

$\dot{m}_g$, lb/min	After Field					Before Field				
	Point 1	Point 2	Point 3	Point 4	Point 5	Point 6	Point 7	Point 8	Point 9	Point 10
NaK Flow = 14.5 lb/min; 0 Gauss										
0.0042	0.061	0.078	0.108	0.096	0.064	0.038	0.104	0.099	0.099	0.046
0.0093	0.154	0.244	0.264	0.245	0.129	0.160	0.264	0.267	0.216	0.189
0.0180	0.272	0.424	0.417	0.376	0.284	0.223	0.377	0.425	0.361	0.241
0.0310	0.296	0.466	0.543	0.490	0.316	0.360	0.512	0.546	0.502	0.386
0.0432	0.371	0.498	0.571	0.559	0.400	0.334	0.524	0.596	0.569	0.368
0.0545	0.487	0.572	0.601	0.571	0.430	0.455	0.554	0.699	0.573	0.488
0.0712	0.501	0.580	0.580	0.625	0.516	0.445	0.580	0.629	0.575	0.481
0.1190	0.486	0.615	0.641	0.590	0.555	0.520	0.580	0.657	0.604	0.498
0.1422	0.509	0.649	0.672	0.631	0.511	0.520	0.621	0.646	0.571	0.496
0.1700	0.545	0.658	0.683	0.625	0.571	0.476	0.644	0.672	0.657	0.520
NaK Flow = 14.5 lb/min; 4300 Gauss										
0.0042	0.071	0.106	0.123	0.120	0.076	0.083	0.144	0.153	0.141	0.096
0.0093	0.146	0.228	0.269	0.232	0.169	0.202	0.268	0.324	0.302	0.225
0.0180	0.227	0.366	0.417	0.387	0.250	0.241	0.428	0.531	0.455	0.272
0.0310	0.343	0.461	0.488	0.489	0.384	0.407	0.559	0.594	0.515	0.411
0.0432	0.404	0.534	0.546	0.526	0.406	0.415	0.600	0.664	0.586	0.433
0.0545	0.438	0.536	0.579	0.561	0.455	0.419	0.605	0.644	0.597	0.458
0.0712	0.398	0.565	0.600	0.577	0.432	0.421	0.627	0.673	0.617	0.422
0.1190	0.501	0.681	0.700	0.670	0.519	0.545	0.684	0.710	0.650	0.576
0.1422	0.535	0.693	0.700	0.695	0.547	0.527	0.709	0.716	0.691	0.555
0.1700	0.549	0.727	0.740	0.696	0.578	0.528	0.703	0.743	0.721	0.566
NaK Flow = 14.5 lb/min; 7840 Gauss										
0.0042	0.063	0.063	0.067	0.063	0.024	0.073	0.119	0.126	0.124	0.098
0.0073	0.121	0.132	0.196	0.136	0.090	0.023	0.217	0.293	0.212	0.083
0.0093	0.132	0.184	0.216	0.188	0.157	0.138	0.275	0.322	0.254	0.167
0.0120	0.259	0.265	0.308	0.272	0.224	0.197	0.354	0.391	0.350	0.208
0.0202	0.213	0.368	0.368	0.365	0.289	0.342	0.471	0.523	0.477	0.282
0.0310	0.319	0.424	0.417	0.396	0.298	0.328	0.524	0.646	0.531	0.363
0.0395	0.332	0.483	0.483	0.493	0.376	0.405	0.588	0.624	0.594	0.390
0.0642	0.415	0.499	0.510	0.475	0.410	0.465	0.600	0.673	0.625	0.453
0.0950	0.448	0.516	0.526	0.529	0.439	0.480	0.654	0.709	0.666	0.488
0.1190	0.470	0.582	0.590	0.552	0.485	0.506	0.661	0.724	0.663	0.488
0.1422	0.422	0.588	0.598	0.540	0.455	0.535	0.674	0.701	0.659	0.576
0.1700	0.453	0.649	0.647	0.616	0.485	0.580	0.710	0.728	0.712	0.551
NaK Flow = 50 lb/min; 0 Gauss										
0.0280	0.194	0.254	0.274	0.271	0.175	0.160	0.232	0.282	0.264	0.228
0.0492	0.226	0.323	0.352	0.355	0.217	0.169	0.368	0.399	0.371	0.214
0.0512	0.266	0.392	0.386	0.330	0.252	0.232	0.383	0.386	0.374	0.270
0.1308	0.372	0.504	0.538	0.482	0.341	0.405	0.490	0.544	0.510	0.416
0.2100	0.454	0.586	0.624	0.586	0.458	0.435	0.574	0.613	0.613	0.439
0.2610	0.484	0.648	0.660	0.582	0.465	0.443	0.601	0.665	0.664	0.429
0.3200	0.510	0.654	0.684	0.656	0.485	0.487	0.668	0.677	0.672	0.515

Table III (Contd.)

$\dot{m}_g$, lb/min	After Field					Before Field				
	Point 1	Point 2	Point 3	Point 4	Point 5	Point 6	Point 7	Point 8	Point 9	Point 10
NaK Flow = 50 lb/min; 4300 Gauss										
0.0155	0.111	0.181	0.191	0.158	0.085	0.069	0.174	0.198	0.181	0.122
0.0295	0.181	0.249	0.292	0.228	0.099	0.205	0.326	0.324	0.289	0.248
0.0503	0.233	0.355	0.366	0.339	0.268	0.252	0.373	0.437	0.373	0.309
0.0937	0.384	0.461	0.480	0.446	0.306	0.390	0.499	0.531	0.485	0.391
0.1210	0.366	0.478	0.516	0.477	0.376	0.425	0.508	0.551	0.530	0.407
0.2100	0.458	0.594	0.621	0.571	0.459	0.441	0.601	0.652	0.574	0.439
0.2610	0.464	0.609	0.651	0.595	0.494	0.503	0.622	0.658	0.626	0.490
0.3200	0.512	0.650	0.675	0.643	0.501	0.491	0.683	0.685	0.658	0.501
NaK Flow = 50 lb/min; 7840 Gauss										
0.0155	0.050	0.074	0.078	0.044	0.038	0.120	0.127	0.151	0.131	0.072
0.0280	0.098	0.208	0.234	0.185	0.075	0.104	0.250	0.308	0.217	0.165
0.0512	0.194	0.318	0.356	0.303	0.179	0.220	0.383	0.452	0.380	0.251
0.1133	0.314	0.421	0.417	0.376	0.296	0.351	0.493	0.506	0.455	0.380
0.1690	0.394	0.464	0.501	0.481	0.375	0.372	0.553	0.579	0.536	0.428
0.2100	0.423	0.517	0.541	0.518	0.424	0.429	0.596	0.605	0.557	0.432
0.2610	0.427	0.601	0.624	0.582	0.432	0.434	0.631	0.669	0.601	0.456
0.3200	0.452	0.587	0.604	0.605	0.471	0.500	0.650	0.667	0.637	0.492

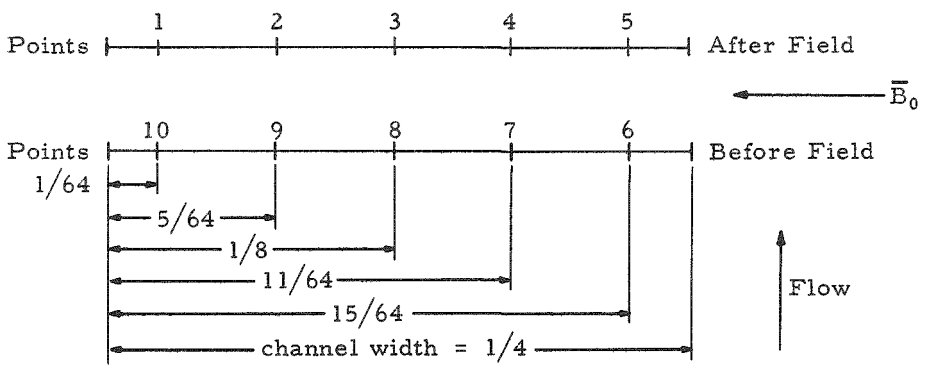

ACKNOWLEDGMENTS

This work was performed by the author in partial fulfillment of the requirements for the degree of Master of Mechanical Engineering in the Graduate School, Syracuse University, with Professor E. E. Drucker as adviser. The work was conducted at the Argonne National Laboratory as part of a program sponsored by the Associated Midwest Universities and was supervised by Dr. Michael Petrick.

The efforts of George Lambert in operating the test facility and assisting in data reduction are gratefully acknowledged. Thanks are also due to Edward Spleha who aided in the construction and shake-down of the apparatus and to M. P. Gats for obtaining the photographs.

BIBLIOGRAPHY

1. Shercliff, J. A., The Theory of Electromagnetic Flow Measurement, Cambridge University Press (1962).

2. Jackson, W. D., Magnetohydrodynamic Channel Flow (unpublished lecture notes), Massachusetts Institute of Technology.

3. Petrick, M., Investigation of Two-phase Air-Water Flow Phenomena, ANL-5787 (1958).

4. Hooker, H. H., and Popper, G. F., A Gamma-ray Attenuation Method for Void Fraction Determinations in Experimental Boiling Heat Transfer Facilities, ANL-5766 (1958).

5. Fluid Meters, Their Theory and Application, ASME Research Publication, 5th Edition (1959).

6. Grace, H. P., and Lapple, C. E., Discharge Coefficients of Small Diameter Orifices and Flow Nozzles, Trans. Am. Soc. Mech. Engrs. (July 1951).

7. Reactor Handbook, Vol. 2, Engineering, AECD-3646, May 1955, Chapter 1.5.

8. Liquid Metals Handbook, Sodium-NaK Supplement, AEC, Washington, D. C. (1955).

9. Elliott, D. G., A Two-fluid Magnetohydrodynamic Cycle for Nuclear-Electric Power Conversion, JPL TR #32-116 (1961).

10. Petrick, M., Performance Characteristics of a Liquid Metal MHD Generator (unpublished, ANL).